**International Erasmus Mundus Master in**
**QUATERNARY AND PREHISTORY**

# Paleo-environmental Reconstruction of the Boca do Chapim and Praia do Areia do Mastro Sequences (Cabo Espichel, Southern Portugal):

Microscopical and geochemical characterizations of Areia do Mastro and Papo-Seco formations (Lower Cretaceous, Barremian)

**PANG, Chun-Han**

**Supervisor: Dr. MARROCCHINO, Elena**

**Co-supervisors: Prof. FIGUEIREDO, Silverio**
**Prof. VACCARO, Carmela**

*Academic year 2021/2022*

# Paleo-environmental Reconstruction of the Boca do Chapim and Praia do Areia do Mastro Sequences (Cabo Espichel, Southern Portugal): Microscopical and geochemical characterizations of Areia do Mastro and Papo-Seco formations (Lower Cretaceous, Barremian)

PANG, Chun-Han

Abstract

Geochemical analysis of sedimentary deposits is a fundamental tool for paleo-environmental reconstructions. In this study, samples from the Lower Cretaceous sequences of the Praia do Areia do Mastro (PAM) and Boca do Chapim (BC) (northern coast of the Espichel Cape, Portugal) were analyzed. Macroscopic and microscopic observations were carried out, associated with calcimetric determinations, L.O.I. measurements, EA-IRMS analysis for the determination of total C and $\delta^{13}C$ content, and ICP-MS analysis for the definition of REE element concentrations to reconstruct their paleo-environmental conditions.

The samples from the PAM site all belong to the Papo-Seco formations, and are mainly composed of sandstones, limestones and mudstones in which organic matter mainly of plant nature is present in varying percentages. The negative $\delta^{13}C$ values of the PAM samples, in agreement with the other data obtained, suggest that these samples formed an estuarine paleo-environment with intertidal lagoon zones. With respect to all the analysis results of this work, three phases of probable paleo-environmental development of the area are confirmed: 1. Open intertidal and lagoon region from low to high and then low temperature. 2. Open lagoon-like region developed into an estuary. 3. Open estuary transformed into closed lagoon.

The BC site's samples that were studied belong to the Areia do Mastro and Papo-Seco

formations. Samples from the Areia do Mastro formation of the BC site show fairly similar characteristics among them, including an almost completely carbonate composition and a micritic texture, while those belonging to the Papo-Seco formation were found to be sandy limestones, mudstones, sandstones and lignite with gypsum. The negative $\delta^{13}C$ values recorded in the samples from this BC site and the lignite sediments with gypsum are also consistent with a lagoon and estuarine paleo-environment. In this case, the data that emerged from this work for the BC site samples allowed us to confirm a probable estuarine to closed lagoon paleo-environmental development with reducing anoxic conditions under climatic conditions varying from low temperature to high temperature.

In conclusion, the microscopic and geochemical characterization of sediments from the Boca do Chapim and Praia do Areia do Mastro sequences has allowed us to investigate the paleo-environmental conditions that characterized this particularly paleontologically important environment during the Barremian (Lower Cretaceous) period.

# Content

# Contents of figures

Chapter II



Chapter III



Chapter IV

Chapter V

Chapter VI

# Contents of tables

Chapter V

# Contents of diagrams

Chapter V

Chapter VI

# I. Introduction

Geochemical analysis of the intertidal and lagoon geological sedimentary deposits is a fundamental tool to reconstruct paleo-environment. The variable contents and composition of the trace earth elements, such as rare earth elements (REE) and stable carbon isotope can be particularly useful to depict temperatures, depths of water, sedimentary detrital inputs and diagenesis in many paleo-environmental studies (Chen and Liu, 2020; Coimbra et al., 2016).

Numerous Mesozoic sites and sequences have been discovered in the same coastline of the Espichel Cape (Portuguese name: Cabo Espichel), since the paleontological sites with dinosaurs and others vertebrates' bones were identified in the 19th century, in the Boca do Chapim Site (Sauvage, 1897). In 1976 were described the first dinosaurs tracks in the Cape (Pedra da Mua and Lagosteiros sites) (Antunes, 1976) and in 2021 were described numerous dinosaurs tracks in the area between Boca do Chapim and Areia do Mastro sites (Figueiredo et al, 2021, 2022b). The Lower Cretaceous sequences of the Praia do Areia do Mastro and the Boca do Chapim have been studied by the Centro Português de Geo-História e Pré-História, Portugal since 1998 (Figueiredo et al., 2015, 2022a, b). Thanks to several investigations on the trace fossils and sedimentary observations (Figueiredo et al., 2021, 2022a, 2022b and references therein), the roughly hypothetical pictures of the Lower Cretaceous lagoon environments of the locations of these two sequences have been illustrated. Paleo-environmental changes, such as sea level and temperature in different formations of the Lower Cretaceous period, however, is still not clear even nowadays, given that several fossilized woods (lignite), terrestrial dinosaurs' fossils and

footprints, aqueous animals' and sedimentary deposits formed by the aquatic mollusks, such as corals and bivalve shells (Figueiredo et al., 2016; 2020) have been collected in various stratum, which are even higher than the current sea level, of these two sequences. A number of the tracks of the fault motions (Aillud 2001; Figueiredo et al., 2015; 2020) in this coastline also show the high opportunity that the sea level had changed frequently in the Lower Cretaceous period.

Microscopic observations and the geochemical analysis, including the calcimetric, loss on ignition (L.O.I.), REE and stable carbon isotope, were utilized to determine the limestone, sandstone, mudstone and marlstone deposits from the the Praia do Areia do Mastro and the Boca do Chapim sequences in this study. The paleo-environmental reconstructions are then looking forward to shed more light on via discussions based on the data in this study.

# II. Geographic settings

Both of the studied locations, the Praia do Areia do Mastro and the Boca do Chapim (Fig. 2.1), are in the Sesimbra municipality (Lusitanian Basin, Portugal), along the most western sector of the Iberian Peninsula. These locations are also both along the same coastline north of the Espichel Cape, which were described numerous Mesozoic vertebrate fossils and dinosaurs' track fossils (Fig. 2.2). The sequence of the Praia do Areia do Mastro (Fig. 2.3) is situated on a coastal cliff (Figueiredo et al., 2022a), with the coordinate approximately 38°26'14" N 9°12'33" W; Boca do Chapim is located at the estuary of the Chapim Stream (Portuguese: Ribeira do Chapim), with the coordinate roughly 38°26'2" N 9°12'43" W (Figueiredo et al., 2022b). This study will focus on the deposits belonging to the lower Cretaceous sedimentary (Barremian) in the sequences of these two locations.

At the paleontological site of the Praia do Areia do Mastro, there are three exposed layers of the formations, namely the Boca do Chapim Formation, (the top layer), Papo-Seco Formation (in the middle layer) and the Areia do Mastro Formation (in the lowest layer). The Areia do Mastro Formation at this site consists of two stages, which are the upper Hauterivian and the lower Barremian. The the Papo-Seco Formation and the Boca do Chapim Formation both belong to Barremian stage. The range of these three stages can date back to the period between approximately 129,4 and 125 million years ago (Figueiredo et al., 2017). The samples collected from this site all belong to the Papo-Seco Formation.

At the paleontological site of the Boca do Chapim, the major exposed layers of the

formations are the Papo-Seco Formation and the Areia do Mastro Formation. In this study, the samples from these two formations both would be analyzed.


Fig. 2. 1, A photo shows the positions of the studied locations, the Boca do Chapim and Paria do Areia do Mastro (modified from a Google Earth image - Modified from a Google Earth image – accessed on July 25th, 2022.).

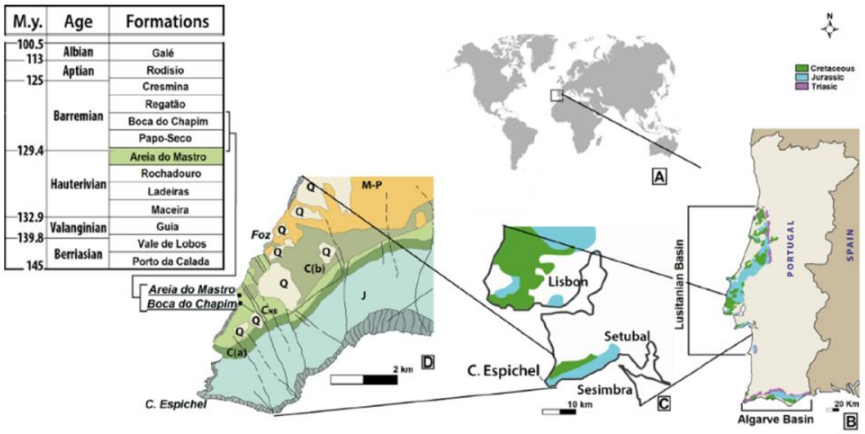


Fig. 2. 2, The map illustrates the positions and geological information of the studied locations. (a) Location of Portugal, (b) Locations and geology of the Lusitanian and Algarve Basin. (c) Locations and geology of the Espichel Cape. (d) Positions and geology of the the Paria do Areia do Mastro, the Boca do Chapim and the neighboring territories. (Figueiredo et al., 2021)

Fig. 2. 3, Photo of the cliff of the Paria do Areia do Mastro site (Figueiredo et al., 2020)

# III. Paleontological and stratigraphic setting

The Lower Cretaceous climate was more humid and warmer than the present climate (Figueiredo et al., 2020), so it made the biodiversity of fauna and flora flourish in that period. The discovery from the Areia do Mastro Formation and the Papo-Seco Formation, which both majorly belong to the Lower Barremian, in the studied two locations near the Espichel Cape show the vivid coastal and estuary/ lagoon-like paleo-environment and ecosystem (Aillud 2001).

At the cliff of the Praia do Areia do Mastro, the Papo-Seco Formation consists of majorly sandstones with fine sands and fine marls (mixing with blackish green clay, lignite and gypsum and so on) from the top to the bottom, except that the PS3 (Papo-Seco Formation bed layer 3) consists of limestone. Every sedimentary bed in the Papo-Seco Formation almost lies horizontally. The mentioned phenomena indicate the lagoon/ estuary type of sedimentary environment (Figueiredo et al., 2016; 2022a) in the Papo-Seco Formation. Otherwise, the Areia do Mastro Formation at this sequence consists of limestone with partially sand, clay and fragments of bivalve shells, and only the top part of this formation exposes above the present sea level. Those evidences illustrate the infralittoral internal type of sedimentary environment (Figueiredo et al., 2021) in the Areia do Mastro Formation. The stratigraphic column of the the Areia do Mastro Formation and Papo-Seco Formation is illustrated in figure 3.1.

Generally, at the sequence of the Boca do Chapim, the compositions of these both formations are similar to those at the cliff's sequence of the Praia do Areia do Mastro.

The exposed Areia do Mastro Formation is composed of the sandy-limestone, and the Papo-Seco Formation is comprised of sandstones and thick fine marls (mixing with blackish green clay, lignite and gypsum and so on) from the top to the bottom. There are numerous cross laminations in the sandstone bedding and some stratums which are full of carbonaceous deposits, which seem to consist of lignite, in the Papo-Seco Formation. Every strata lies horizontally with slightly oblique caused by the fault motions (Figueiredo et al., 2022b). The marl, sandstone with cross lamination and those mentioned horizontal stratums have also depicted the lagoon/ estuary type of sedimentary environment (Aillud 2001).

The fossils belonging to the the organisms that lived in marine, coastal and intertidal ecosystems, which were collected in the two studied sites can also be proved that the coastal paleo-environment (including in lagoon, estuary and infralittoral internal environments).

At the Boca do Chapim and Areia do Mastro, numerous investigations and fieldworks have made the remains of several terrestrial vertebrates living around coastal or intertidal zones found from the 19th century to nowadays. For example, the collected fossils include in several large dinosaurs' (ornithopods, theropods and sauropod dinosaurs), turtles', and crocodiles' bone and teeth (Lapparent and Zbysewski, 1957; Figueiredo et al., 2015); the photos are shown in the figure 3.3 and 3.4. According to the published essay (Figueiredo et al., 2022b), the footprints of several dinosaurs were also discovered in the dried estuary region of the Boca do Chapim sequence's the Papo-Seco Formation.

At the Praia do Areia do Mastro, the fossil fragments of the pterosaurs, crocodiles,

turtles and dinosaurs were discovered during roughly this twenty decades investigation and research works (Figueiredo et al., 2020). During the excavation work of its Papo-Seco Formation, invertebrate animal's fossils, particularly bivalves and gastropods, were easily found. The vertebrate animals' fossils, such as fish's (Lepidotes), the crocodylomorphs' (Anteophthalmosuchus), pterosaurs' (Ornitocheiridae and Ctenochasmatoidea) teeth and dinosaurs' (Baryonyx sp., Cf. Mantellisaurs sp. ornithopods and sauropods indet.) not only bones but also teeth were also abundantly discovered and the photos are shown in the figure 3.3 and 3.4, according to the published essays (Figueiredo et al., 2015, 2020, 2016). The types of fossils found at the Praia do Areia do Mastro are generally similar to those at the Boca do Chapim. During the research work of its Areia do Mastro Formation, not only the fossils of the invertebrate's shells and turtles shells fragments, were collected, but also the dinosaur's tracks (Fig. 3.5) were discovered. Based on the mentioned characteristics of the paleo-environmental sedimentary types and the various fossils and animals' remains, a vivid picture of the lower Cretaceous coastal and lagoon ecosystems and food chains can be illustrated (Fig. 3.6).

Sediments in estuaries and lagoons generally, majorly consist of marl and sand with the fluvial channels' traces, while those in the underwater coast region consist of limestone and sand. In the Papo-Seco Formation of the sequences of the Praia do Areia do Mastro and the Boca do Chapim, the compositions of some layers are limestone or sandy-limestone, and bivalves' and gastropods' fossils also exist in these layers. These phenomena point out the possibility that the sea level changed frequently (Figueiredo et al., 2020) during the period of the Papo-Seco Formation in these two locations.

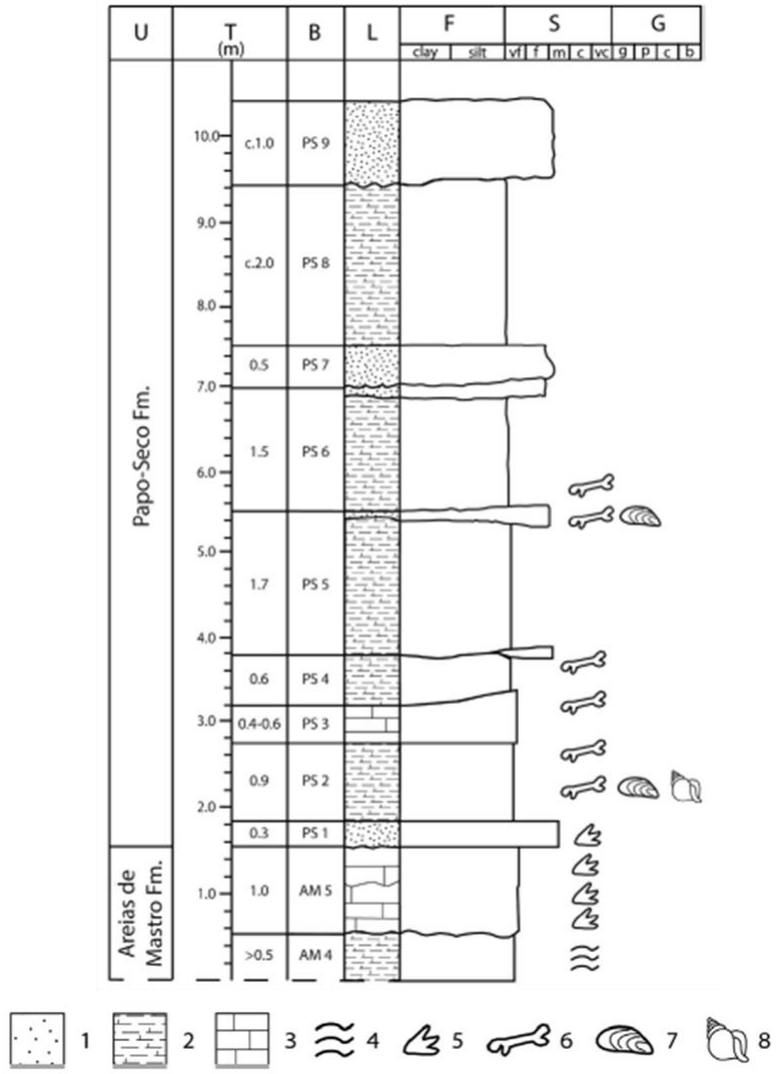


Fig. 3. 1, The stratigraphic column of the Praia do Areia do Mastro site. The meanings of various icons labeled by different numbers and letters in this figure are shown below –1. sandstone; 2. marl; 3. limestone; 4. lamination; 5. dinosaurs' footprint fossils; 6. dinosaurs' bone or tooth fossils; 7. bivalves; 8. gastropods; U. lithostratigraphic unit; T. thickness; B. bed reference; L. Lithology; F. fines; S. sand; G. gravel. (Figueiredo et al., 2022a)

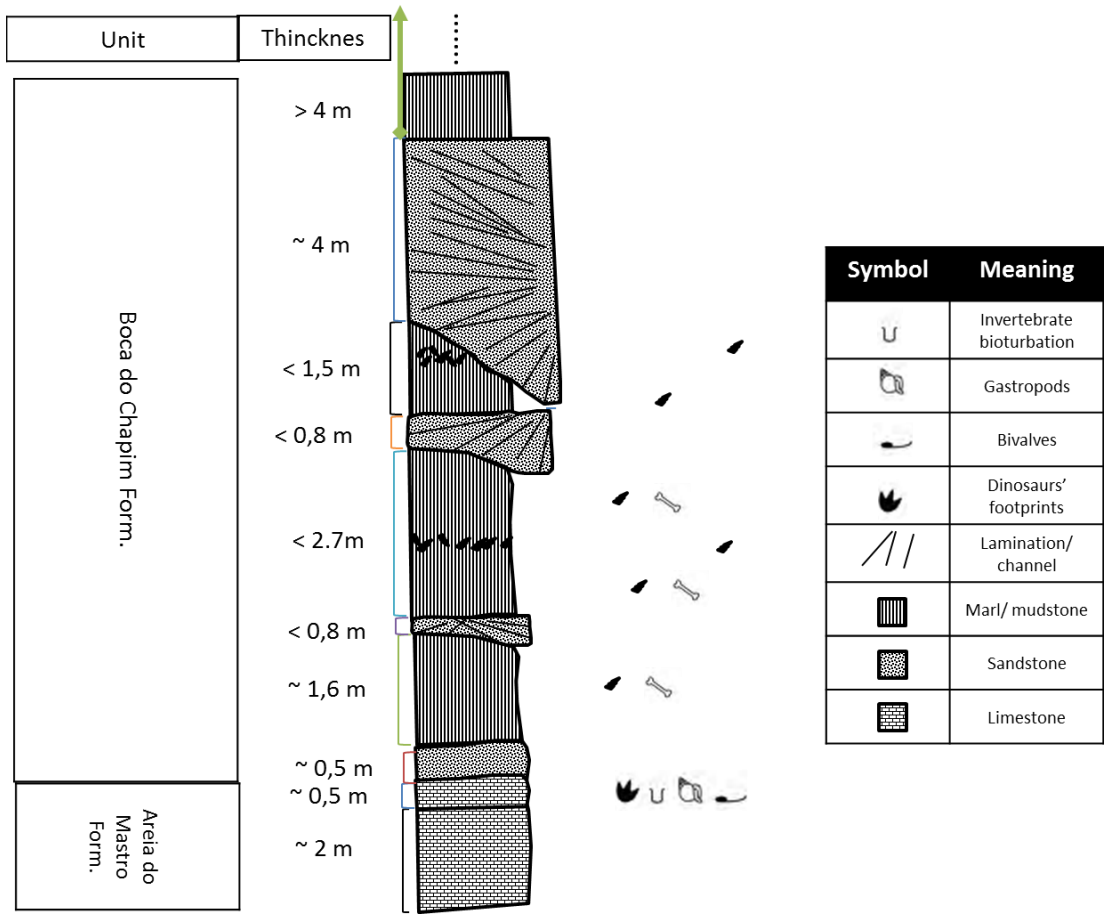


Fig. 3. 2, The sketched stratigraphic section of the the Boca do Chapim site. (This sketch was drawn by the author and based on the unpublished data of Cunha's unpublished data and the work of Figueiredo et al. in 2022b)

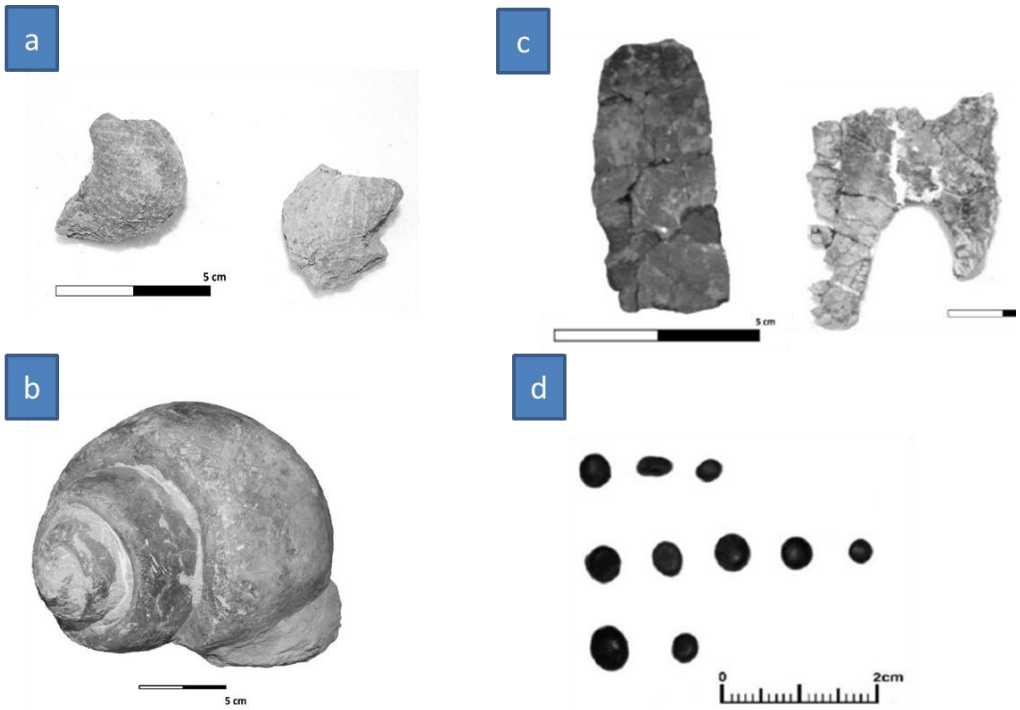


Fig. 3. 3, The Mesozoic marine animals' fossils collected in the studied areas. (a) Shells of a bivalve (*Nipponomaia sp.*), (b) shell of a gastropod (Naticidae) (c) bone of turtles (the left is the costal plate position and the right is the plastron position) and (d) teeth of the fish, *Lepidotes.* (Figueiredo et al., 2016)

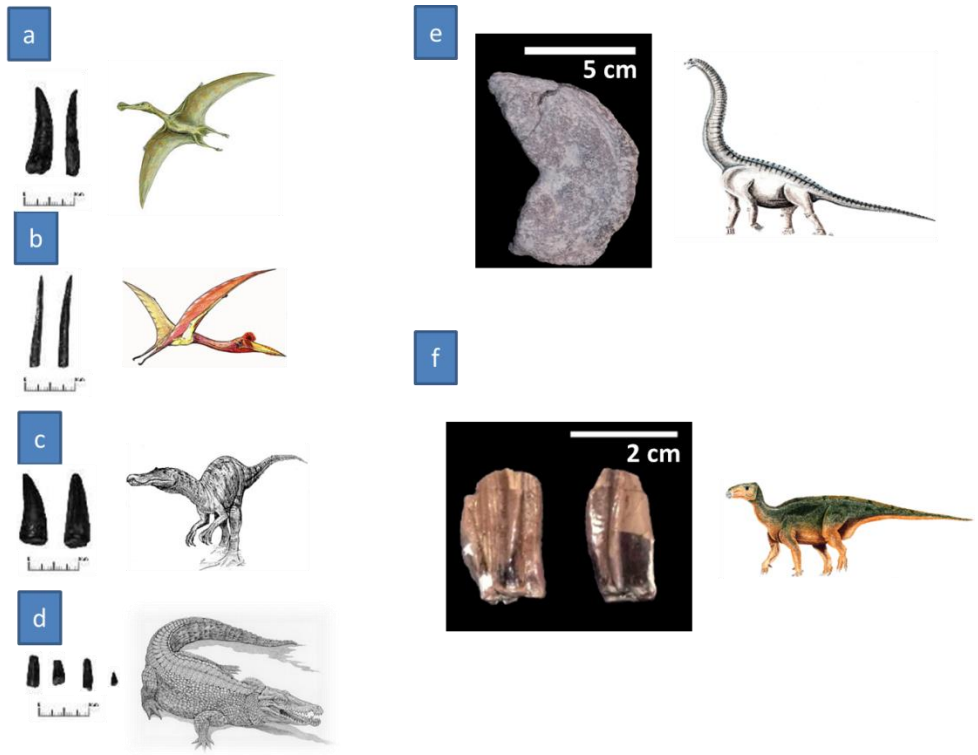


Fig. 3. 4, The fossils, which were collected in the studied areas, of the teeth and bones of the Mesozoic animals living in the coastal and lagoon regions. (a) The teeth of Ornithocheiridae, (b) teeth of Ctenochasmatoidea, (c) teeth of *Baryonyx*, (d) teeth of the crocodylomorph, *Anteophthalmosuchus sp.*, (e) a piece of vertebra of sauropod, and (f) teeth of Styracosterna indet. (Figueiredo et al. 2015, 2016)

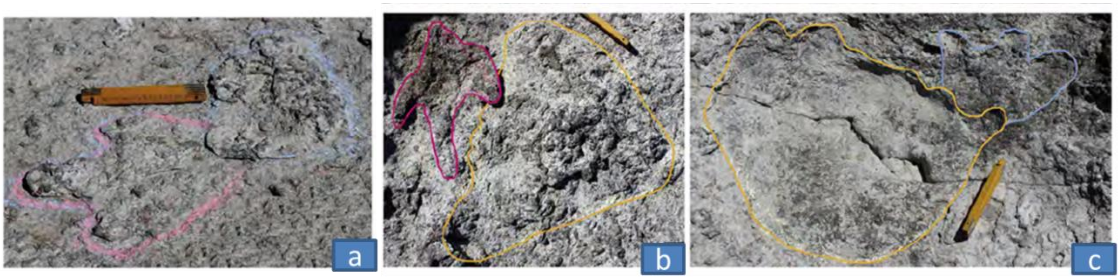


Fig. 3. 5, Dinosaurs' footprints discovered in the studied areas. (a) Footprints of theropod (in the red circle) and ornithopod (in the blue circle), (b) footprints of theropod (in the red circle)/sauropod (in the yellow circle), and (c) footprints of sauropod (in the yellow circle) and ornithopod (in the blue circle) (Figueiredo et al., 2022b)

Fig. 3. 6, A hypothetical picture of the ecological environment in the early Cretaceous of the Espichel Cape region. (art of Fernanda Sousa, in Figueiredo et al., 2022b)

# IV. Materials and methods

## IV.1 Sample collection

The samples in this study were collected by Prof. Silvério Figueiredo (Polytechnic Institute of Tomar; Centro Português de Geo-História e Pré-História) and by Prof. Pedro P. Cunha (University of Coimbra).

The six samples collected from the Praia do Areia do Mastro site all belong to the Papo-Seco (PS) Formation, namely the PS1, 2, 3, 5, 7, and 8 (Fig. 4.1.1). Those samples have different lithology which can be roughly identified by macroscopic examination. The stratigraphic section of this site is shown on figure 3.1.

The eleven samples collected from the Boca do Chapim site (Fig. 4.1.2) belong to the Areia do Mastro Formation and the Papo-Seco Formation in different stratums. The samples are labeled as no. (Number) 1 to 11. Stretched stratigraphic section of this site is shown on the figure 4.1.3.

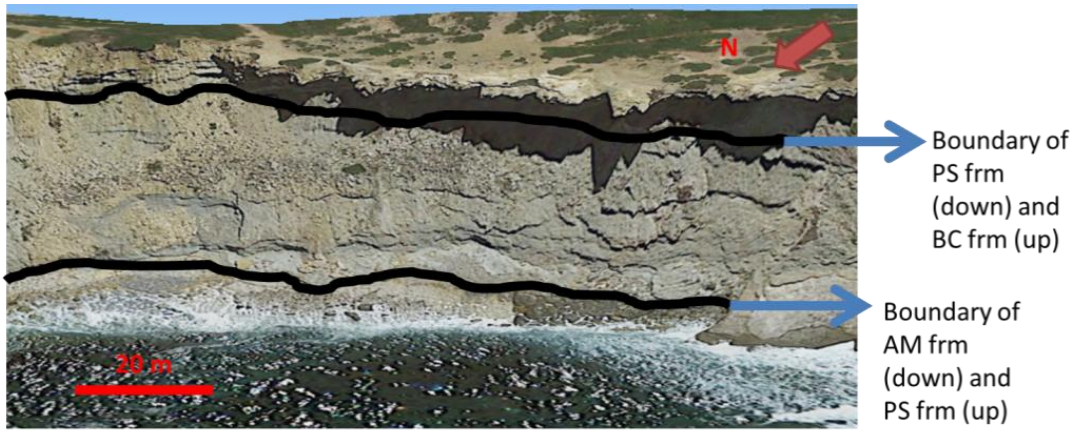


Fig. 4.1. 1, The photo of the cliff of the Praia do Areia do Mastro site where the samples, PS1, 2, 3, 5, 7 and 8 were collected. (Modified from a Google Earth image – accessed on August 8th, 2022)

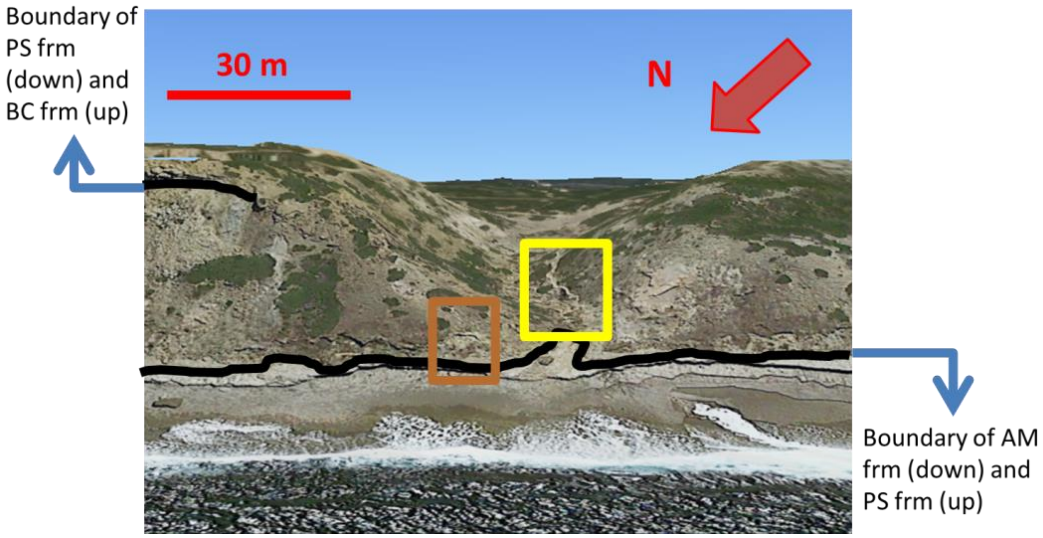


Fig. 4.1. 2, The photo of the cliff of the Boca do Chapim site, where the samples no. 1 to 11 were collected. The place marked by the yellow rectangle is where the samples no. 1 to 5 were collected; the brown rectangle locates where the samples no. 6 to 11 were collected. (Modified from a Google Earth image – accessed on August 8th, 2022)

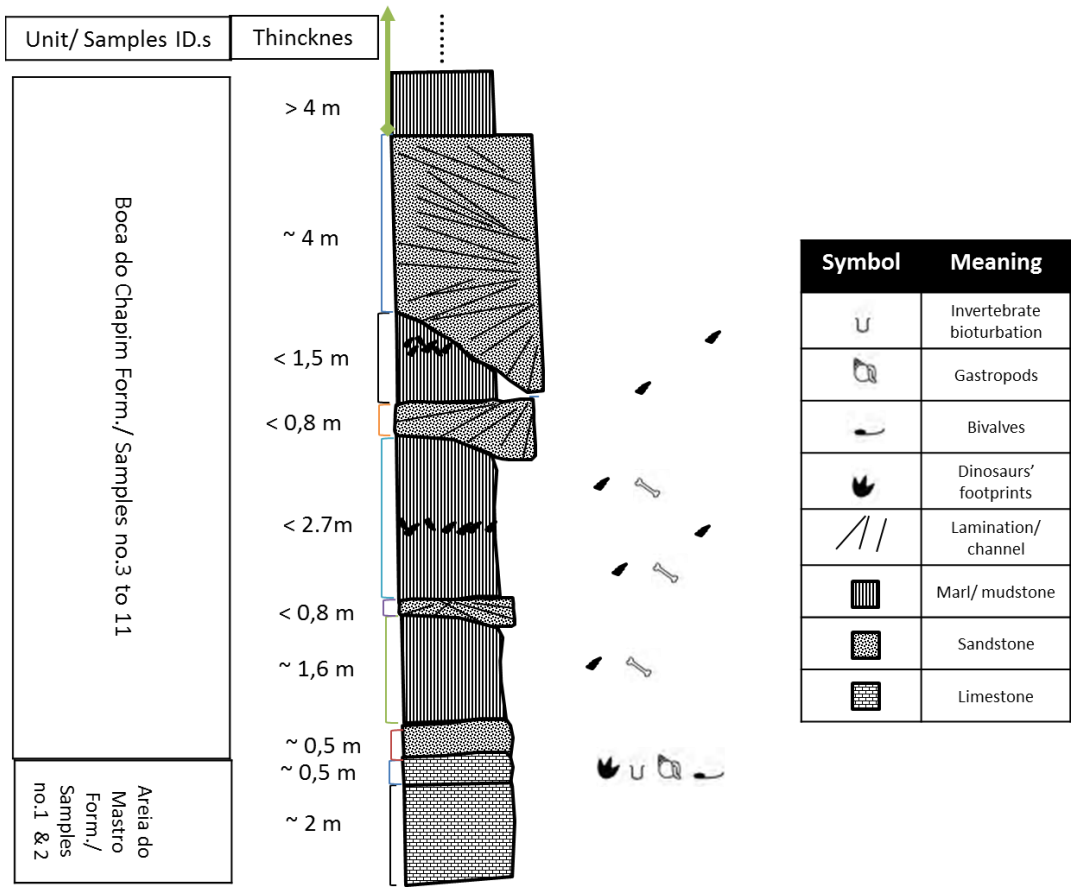


**Fig. 4.1. 3, The sketched stratigraphic column of the Boca do Chapim site shows the stratum where the samples belong (This sketch was drawn by the author and based on the unpublished data of Cunha's unpublished data and the work of Figueiredo et al. in 2022b)**

## IV.2 Sample preparation

The samples, which are listed in the bullet points below, were sliced by a stone cutting machine with circular saw, in order to get their fresh cross-sections for the further observation through the stereomicroscope:

- Samples from the Praia do Areia do Mastro site – Strata PS 1, 2, 3, 5, 7, and 8
- Samples from the Boca do Chapim site – samples no. 1, 2, 3, 4, 5, 6, 8, 9, 10, and 11

The sample no. 7 from the Boca do Chapim was not sliced by the machine, since its structure is too weak to be cut or sliced.

In order to do the further instrumental analysis, all of the samples should be modified to be powder. Therefore, all the sliced samples were crushed by a stone crusher to be crispy small stones or powders. After crushing these samples, they were then ground to be fine powders by an electric mortar grinder. The modified samples are shown in the list below:

- Samples from the Praia do Areia do Mastro site– Strata PS 1, 2, 3, 5, 7, and 8
- Samples from the Boca do Chapim site – samples no. 1, 2, 3, 4, 5, 6, 7, 8, 9, 10, and 11

All the preparations, descripted in section IV.2, were operated in the Department of the Physics and Earth science, the University of Ferrara.

## IV.3 Taking pictures of the samples in macroscopic view

All of the samples were taken photos by the Canon® high resolution camera before further modification and analysis. Because for the further research work, the samples would be broken by modifications, such as grinding and polishing, using photos to record the original states of the raw samples is necessary for this study.

Expect that the photo of the non-sliced sample of the sample No. 7 from the Boca do Chapim site was only taken because of its weak structure; all of the sliced and non-sliced samples were taken photos. The photos of the non-sliced samples would be used to depict the situations of the raw materials, and the sliced samples would be used to show that of the fresh cross-sections of the raw materials.

The process, descripted in section IV.3, was operated in the Department of the Humanities Studies, the University of Ferrara.

## IV.4 The stereomicroscope observation

Micromorphology of the samples can be observed through the stereomicroscope.

In order to make the surface of all the samples easy to be observed by a stereomicroscope, all the samples were soaked in resin, and after the resin dried, all the samples in the dried resin were sliced by the saw to get their fresh cross-sections without covered by the dust or impurities.

The OPTIKA SZ-CTV optical stereomicroscope (10x, 20x, 30x, and 40x in

magnification) was utilized to observe the micro-morphological texture of the samples.

The preparation work and analysis, descripted in section IV.4, were operated in the Department of the Physics and Earth Science, the University of Ferrara.

## IV.5 The LOI determination

In this study, the LOI (Loss on Ignition) analysis was used to evaluate the amount of volatile content in all the samples at high temperature (generally in the range from 500 to 1000℃). The weight differences of the volatile content at 500℃ and 1000℃ are approximately correlated to the weight percentage of the organic matters and inorganic carbon matters content, respectively in this study.

This analysis was operated by following steps –

1. 0,50 g of the ground powder of the samples were first dried in an oven at 110℃ and then placed in the ceramic crucibles.
2. The dried samples with the crucibles were subjected to a temperature of 500℃ for one day.
3. After calcination at 500℃ for a day, the heated samples were measured and recorded.
4. Then, the samples with the crucibles were subjected again to a temperature of 1000℃ for one day.
5. After calcination at 1000℃ for a day, the heated samples were measured and recorded again.

This analysis work was operated in the Department of the Physics and Earth Science, the University of Ferrara.

## IV.6 The calcimetric analysis

In order to roughly understand amount of the calcium carbonate contents in all the samples, the calcimetric analysis was used to approximately determinate these. The theory of this analysis is that after the chemical reaction between carbonate substances and hydrochloric acid, the carbon dioxide gas will be produced. This reaction can be illustrated by the chemical formula below –

$$CaCO_{3\,(s)} + 2HCl_{(aq)} \rightarrow CaCl_{2\,(s)} + H_2O_{(l)} + CO_{2\,(g)}$$

Thus, the rough amount of the carbonate competitions can be understood by the determination of the pressure's or volume's percentage change of the produced carbon dioxide gas. Before the analysis of the studied samples, the pure calcium carbonate with the same weight as the samples were used to react with the hydrochloric acid with the same concertation and volume, in order to obtain the calibration values. If the volume of the carbon dioxide produced by the reaction of the calibration is the symbol, $V_{cal}$ and counterpart produced by the reaction of the sample for the same time is the symbol, $V_{sam}$ (both reaction times are also the same), then the formula to calculate the carbonate compositions' percentage, $\%CaCO_3$, of the sample can be depicted as –

$$\%CaCO_3 = \frac{V_{sam}}{V_{cal}} \times 100\%$$

For the method of the calcimetric analysis in this study, all the 0,500 g ground powder samples were individually mixed with the 5,0 mL of 10(v/v)% hydrochloric acid in a

closed container to allow the reaction to proceed. An RS electronic gas-volumetric calcimeter (Fig. 4.6.1) was determined the volume change of the carbon dioxide while the reactions proceeded through three-step measures (60, 180, and 900 s from starting time of the reaction).

This analysis work was operated in the Department of the Physics and Earth Science, the University of Ferrara. The author would like to thank Dr. Umberto Tessari who is responsible of the laboratory.

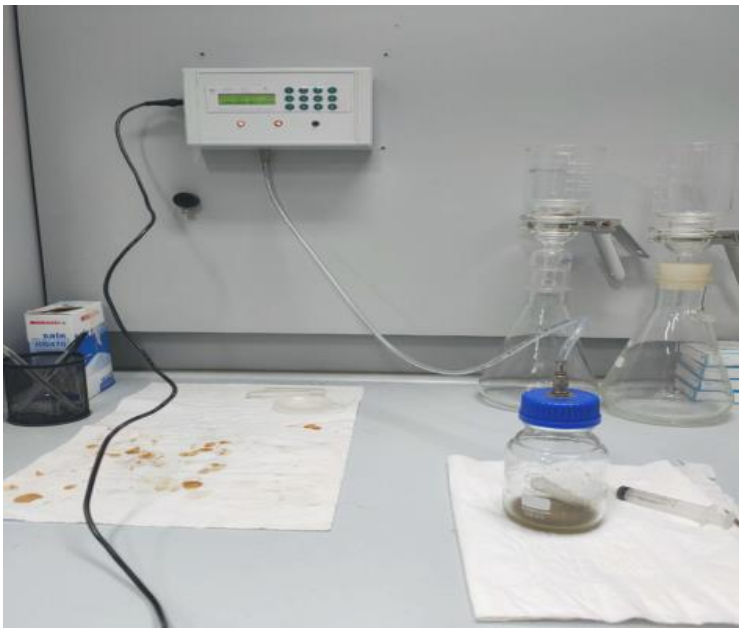

**Fig. 4.6. 1, The photo of the entire system (including in RS electronic gas-volumetric calcimeter) of the calcimetric analysis**

## IV.7 The EA-IRMS analysis

In this study, the isotope ratio mass spectrometry with the elementar vario Micro Cube (EA-IRMS) analysis was used to determine the weight percent of the stable isotopic carbon composition ($^{13}C$ and $^{12}C$) of the different carbon pools and the ratio (reported in parts per thousand) of the $^{13}C$ to $^{12}C$ in all the samples. The ratio of the $^{13}C$ to $^{12}C$ is calculated by the formula below –

$$\delta^{13}\mathrm{C}\ (/‰) = \left[\frac{\left(\frac{12\mathrm{C}}{13\mathrm{C}}\right)_{sample}}{\left(\frac{12\mathrm{C}}{13\mathrm{C}}\right)_{standard}} - 1\right] \times 1000$$

For the EA-IRMS analysis, the samples were modified, vaporize and purified by the following steps —

1. The ground samples were introduced in tin capsules that are wrapped and weighed.
2. The capsules (with the capacity up to the 10 mg of sample) with the ground samples were introduced into the Vario Micro Cube auto-sampler to let the flash combustion (the temperature up to 1050℃) oxidize them to be form the $CO_2$ gas in a sealed quartz tube (with copper oxide grains as a catalyst and exceeding high purified (6-grade purity) $O_2$ gas.
3. The formed $CO_2$ gas, which was carried by the dry purified (5-grade purity) He gas, passed a water trap filled with Sicapent® to remove the potential moisture completely.

The vaporized, purified samples were quantitatively determined on a thermos-conductivity detector (TCD), and then measured the carbon isotopic ratios by

the IRMS instrument (ISOPRIME 100 IRMS operating in continuous flow mode).

The detection of the distinct isotopic masses of the sample were compared to those of 5-grade purified reference $CO_2$ gas, which has been calibrated using a series of reference materials, in turn, calibrated against the IAEA international standards, such as the limestone JLs-1 (Kusaka and Nakano 2019), the peach leaved the NIST SRM1547 (Dutta et al. 2006), the Carrara Marble (calibrated at the Institute of Geoscience and Georesources of the National Council of Researches of Pisa), and the synthetic sulfanilamide provided by the Isoprime Ltd.

Mass peaks were recalculated as isotopic ratios by the Ion Vantage software package. The elemental precision, estimated by repeated standard analyses, and accuracy, estimated by the comparison between reference and measured values, were on the order of 5% of the absolute measured value. The uncertainty increased for contents approaching the detection limit (0.01 g/kg). The results of carbon isotope ratios were expressed in the standard (δ) notation in per mil (‰), relative to the international Vienna Pee Dee Belemnite (V-PDB) isotope standard (Gonfiantini, Stichler, and Rozanski 1995). The $\delta^{13}C$ values were characterized by an average standard deviation of ± 0.1‰ defined by repeated analyses of the mentioned standards.

The preparation work and analysis, descripted in section IV.7, were operated in the Department of the Physics and Earth Science, the University of Ferrara.

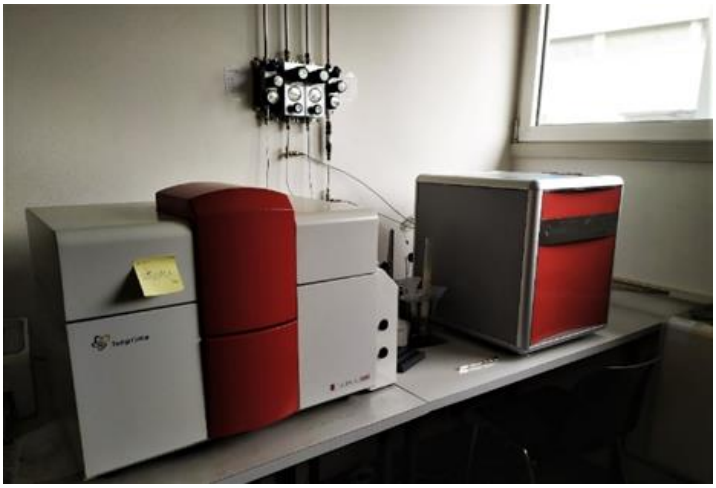

Fig. 4.7. 1, The photo of the EA-IRMS instrument. The right part is the 'Elementar Vario Microcube' elemental analyser, and the left part is the ' ISOPRIME 100 IRMS' mass spectrometer

Fig. 4.7. 2, The photo of tin capsules used for IRMS analysis

## IV.8 The ICP-MS analysis

In this study, the ICP-MS (Inductively Coupled Plasma Mass Spectrometry) analysis was used to determine the amount of the REE (rare earth elements) contents in all the samples.

For the ICP-MS analysis, solutions of the samples (except for the samples which contain organic matters, namely the sample No.7 and 10 from the Boca do Chapim site) were prepared by the following steps in order to remove the impurities, such as fat, protein, organic and inorganic carbon species, silicate matters and so on, in the samples –

1. All the powders of the ground samples (0,200 g) were placed in the PTFE beakers to react with 6 mL of 40% hydrofluoric acid and 3 mL of 65% nitric acid at room temperature for 24 h.
2. After reacting for 24 h, the solutions of the samples were placed on a heating plate at 195℃ to make the solvent of the samples' solutions evaporate until only the dried samples were left in the beakers.
3. The dried samples in the beakers reacted with 3 mL of 40% hydrofluoric acid and 3 mL of 65% nitric acid on the heating plate at 195℃ until all of the solvents in the beakers evaporated to leave the dried samples.
4. The dried samples in the beakers reacted with 4 mL of 65% nitric acid on the heating plate at 195℃ until all of the solvents in the beakers evaporated to leave the dried samples.
5. The dried samples were mixed with 2 mL of 65% nitric acid at room temperature and then put into 100 mL volumetric flask. (Ultrapure water, which was obtained through the milli-Q purification system (Millipore® Corp., Bedford, MA, USA), was used in this preparation).
6. The solutions which were prepared by the previous steps were then kept in tubes for the ICP-MS analysis.

For the ICP-MS analysis, solutions of the sample No.7 and 10, which contain

numerous organic matters,were prepared by the following steps in order to remove the impurities, such as fat, protein, organic and inorgainc carbon species, silicate matters and so on, in the samples –

1. The powders of the ground samples (0,200 g) were both placed in the Teflon beakers, and then added 4 ml of nitric acid and 3 ml of hydrogen peroxide at room temperature for 24 hours.
2. After reacting for 24 h, the solutions of the samples were placed on a heating plate at 130℃ to make the solvent of the samples' solutions evaporate until only the dried samples were left in the beakers.
3. The dried samples in the beakers reacted with 2 ml of hydrogen peroxide and 3 mL of 65% nitric acid on the heating plate at 130℃ until all of the solvents in the beakers evaporated to leave the dried samples.
4. The dried samples in the beakers reacted with 3 mL of hydrogen peroxide on the heating plate at 130℃ until all of the solvents in the beakers evaporated to leave the dried samples.
5. Ultrapure water, which was obtained through the milli-Q purification system (Millipore® Corp., Bedford, MA, USA), was added to the volumetric flask with the mixture of the samples and 2 mL of the 65% nitric acid until the volumes of all the solutions were 100 mL in total.
6. The solutions which were prepared by the previous steps were then kept in tubes for the ICP-MS analysis.

The REE, namely Ce, Ga, Hf, La, Nb, Nd, Ni, Pb, Rb, Sr, Th, Y, Zr, etc. were determined by the ICP-MS instrument (Thermo Fisher Scientific, Waltham, MA, USA). Accuracy and precision of result of this analysis was checked by certified

international sediments standard (the *HISS-1, National Research Council, Canada*).

The preparation work and analysis, descripted in section IV.8, were operated in the Department of the Physics and Earth Science, the University of Ferrara. The author would like to thank Dr. Renzo Tassinari who is responsible of the laboratory.

# V. Results

## V.1 Brief introduction of sedimentary rocks

Sedimentary rocks are types of rocks formed on or near the Earth's surface. These types of rocks are generally formed by common geological process, such as erosion, weathering, dissolution, precipitation and lithification at normal surface temperatures. The components of sedimentary rocks can be either organic (for example, plants' and animals' remains) or inorganic (for example, marine animals' broken up pieces of other rocks).

Grain sizes of sediments and detritus of sedimentary rocks are a vital textural parameter of clastic rocks. Those sediments can be roughly classified as gravel (>2 mm), sand (2,0–0,062 mm), and clay (0,062 – 0,004 mm), depending on their mean grain sizes (Fig. 5.1.1). Chemical characteristics are also the other important parameter to classify the sediments, and the chemical information may further depict the diagenesis and detrital inputs of them. Sediments with a variety of ratios of different grain sizes and chemical characteristics form various sedimentary rocks (Fig. 5.1.2).

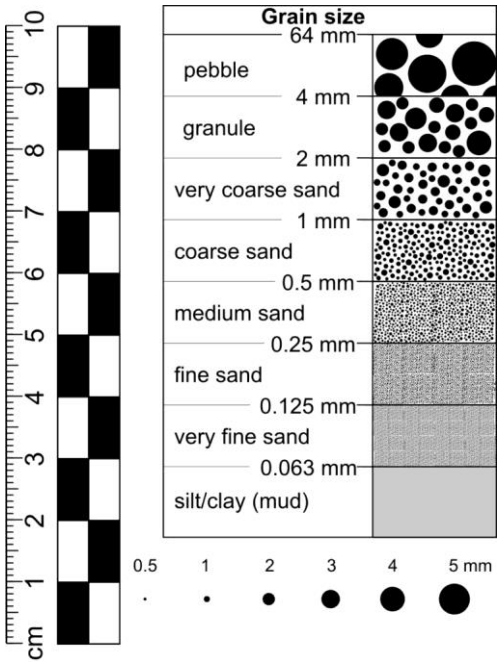


Fig. 5.1. 1, A classification chart of the sediments based on their grain sizes. (Papeschi, 2022)

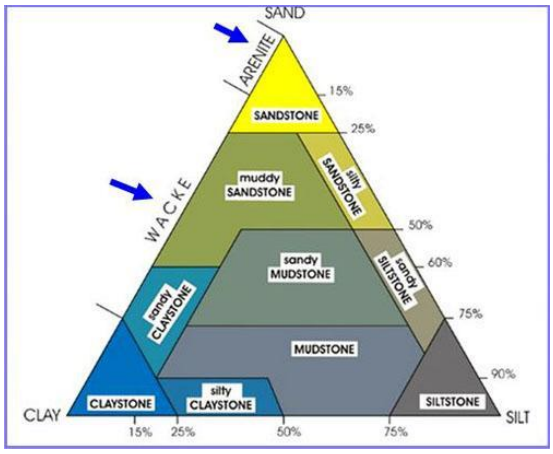


Fig. 5.1. 2, A classification diagram for Terrigenous Sedimentary Rocks based on ratios of the sediments with various grain sizes. (Lindholm, 1988)

In this chapter, the information of the grain sizes of the samples would be illustrated by high resolution camera's and optical stereomicroscope's photos; the chemical characteristics would be shown by the results of the L.O.I, calcimetric, EA-IRMS and ICP-MS analysis.

## V.2 Macroscopic and microscopic observations

### V.2.1 The samples of the Praia do Areia do Mastro site

The six samples (PS1, 2, 3, 5, 7 and 8, which are pointed out in the figure 5.2.1.1) of the Praia do Areia do Mastro site all belong to the Papo-Seco formation (PS Form.). According to Aillud (2001) and Figueiredo et al. (2020, 2022a), the Papo-Seco Formation (PS Form) in this site, located about 1.5 km north, in along the Espichel Cape coastline, consist of majorly silty gray marls, mudstones, grey carbonate silts and lenses of fine, ribbon shaped, bioturbated, clastic sand. Compared to the description of the mentioned publications in this paragraph, the samples' photos for macroscopic and microscopic observations are shown on the paragraphs below in the order from the top layer to the bottom one–

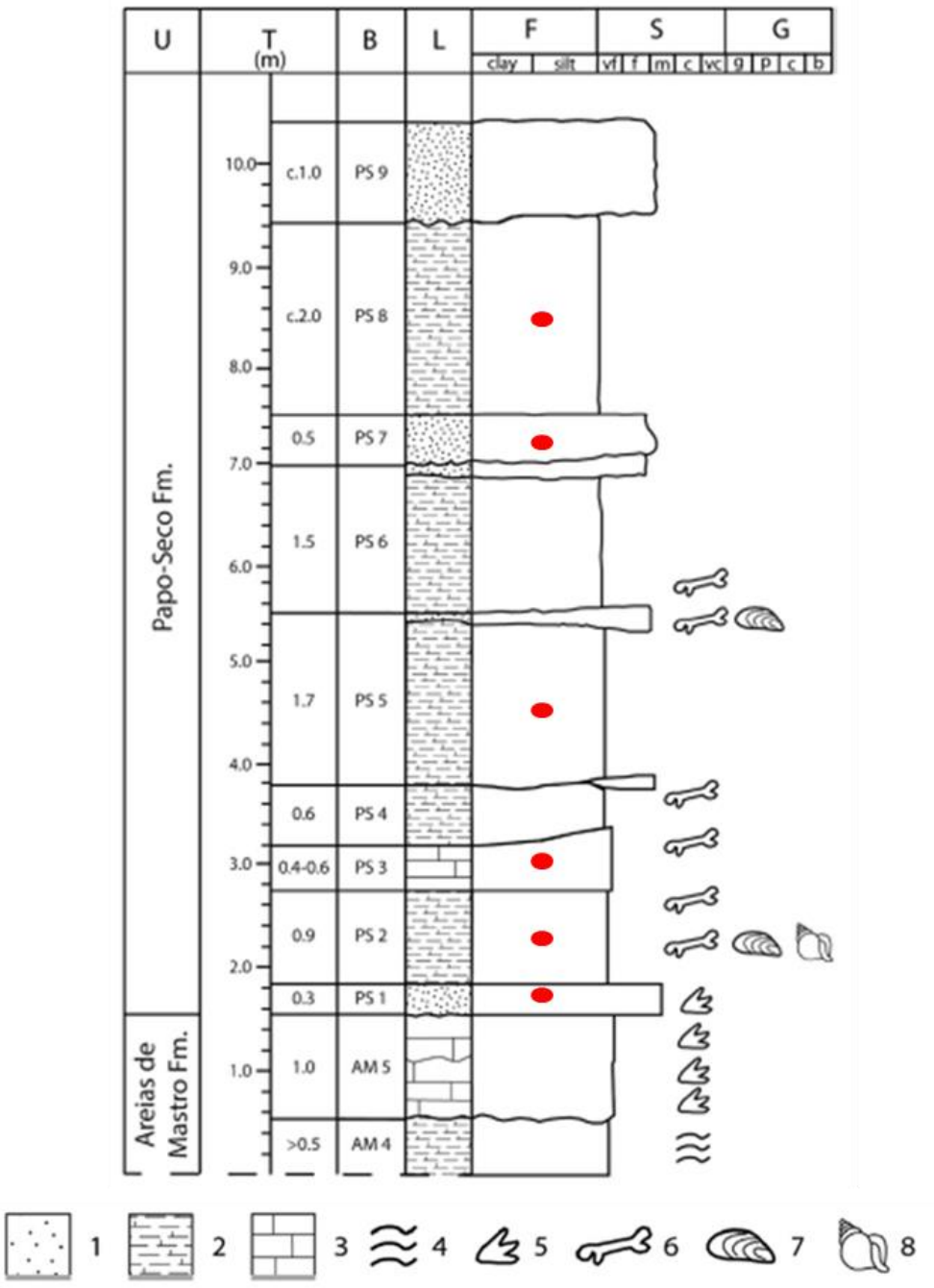


Fig. 5.2.1. 1, The stratigraphic section of the Praia do Areia do Mastro site, with the labels to show the samples' collected stratum. The meanings of various icons labeled by different numbers and letters in this figure are shown below –1. sandstone; 2. marl; 3. limestone; 4. lamination; 5. dinosaurs' footprint fossils; 6. dinosaurs' bone or tooth fossils; 7. bivalves; 8. gastropods; U. lithostratigraphic unit; T. thickness; B. bed reference; L. Lithology; F. fines; S. sand; G. gravel. (Figueiredo et al., 2022a)

Sample PS8 (Fig. 5.2.1.2a) macroscopically appears gray to dark green in color. The color is quite homogeneous; the surface of the sample is dusty to the touch and slightly resistant. It is muddy, when mixed with or touched by water. The microscopic observations (Figure 5.2.1.2b to f) of the sample PS8 show a gray binder with a size smaller than 0,2 mm, the presence of few quartz minerals with dimensions around 0,6-0,8 mm, a few feldspars milky colored and a few muscovite. It also presents a small amount of organic matter black/dark brown colored (Figueiredo's work published in 2022a) suggested that it should be lignite). The sample PS8 could be classified as a mudstone with a fraction of fine sand.

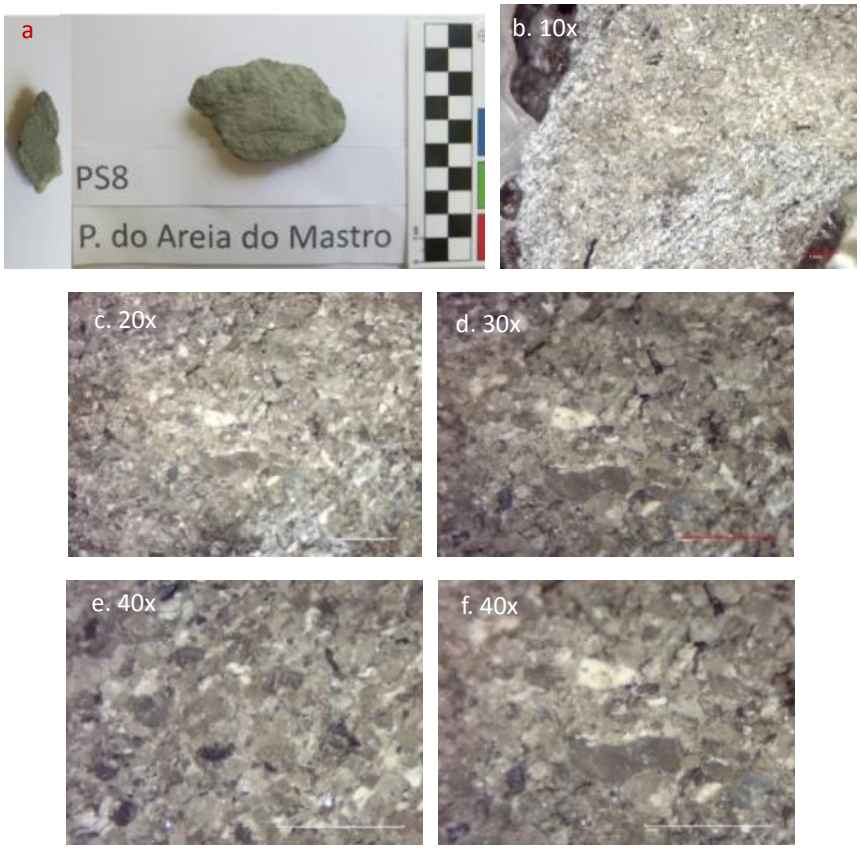


**Fig. 5.2.1. 2, Macroscopic (a) and microscopic (b to f, labeled with the magnification) photos of the sample PS8.**

Sample PS7 (Fig. 5.2.1.3a) macroscopically appears gray with dark green in color. The color is slightly not homogeneous; the surface of the sample is sandy to the touch and not resistant. The microscopic observations (Figure 5.2.1.3b to f) of the sample PS7 show that it is composed by a carbonatic limestone fraction associated with a fraction mainly composed by quartz, feldspar with irregularly shaped and size around to 0,4-0,8 mm and some clay minerals. It is also present a fraction of organic matter with dark brown color. It could be presumed that the sample PS7 is a polygenic limestone with a silty terrigenous fraction and a few minerals typical of the medium sand.

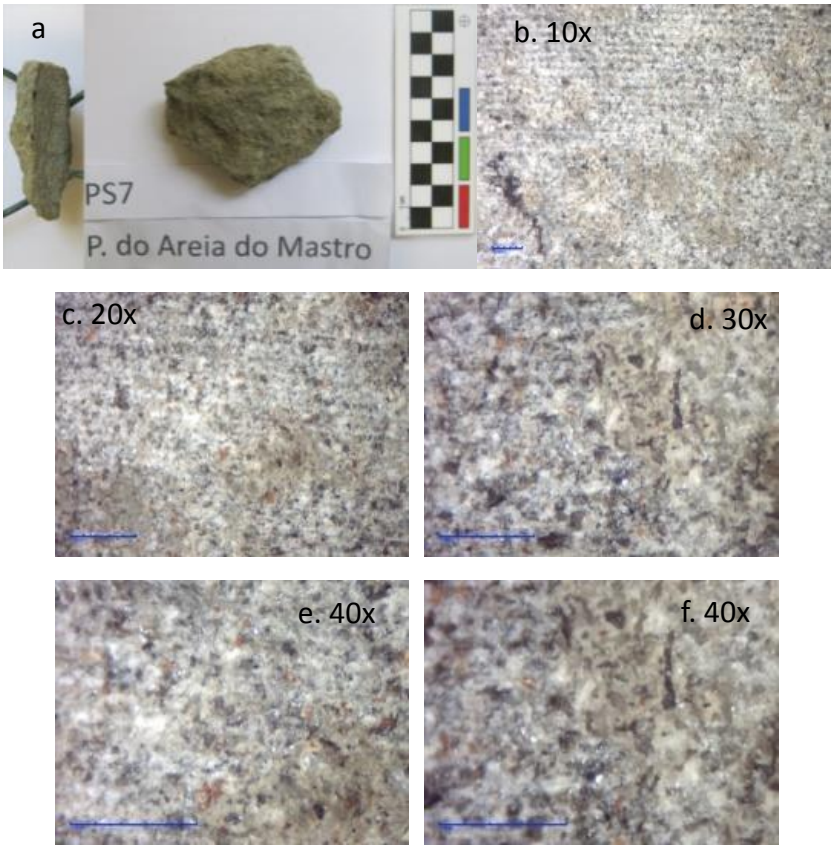


**Fig. 5.2.1. 3, Macroscopic (a) and microscopic (b to f, labeled with the magnification) photos of the sample PS7.**

Sample PS5 (Fig. 5.2.1.4a) macroscopically appears khaki in color. The color is very homogeneous; the surface of the sample is dusty to the touch and resistant. It is muddy, when mixed with or touched by water. The microscopic observations (Figure 5.2.1.4b to f) of the sample PS8 show that the sample is mainly composed of a carbonatic mud fraction associated with a silty fraction composed of terrigenous minerals. A few khaki and black particles with a size roughly equaled to 0,2 mm are filled by a significant white carbonate binder with the size much smaller than 0,02 mm. The grain sizes of the particles in the sample PS5 depict that the sample could be presumed as a limestone with a significant part of terrigenous fractions present both as fine sand and mud.

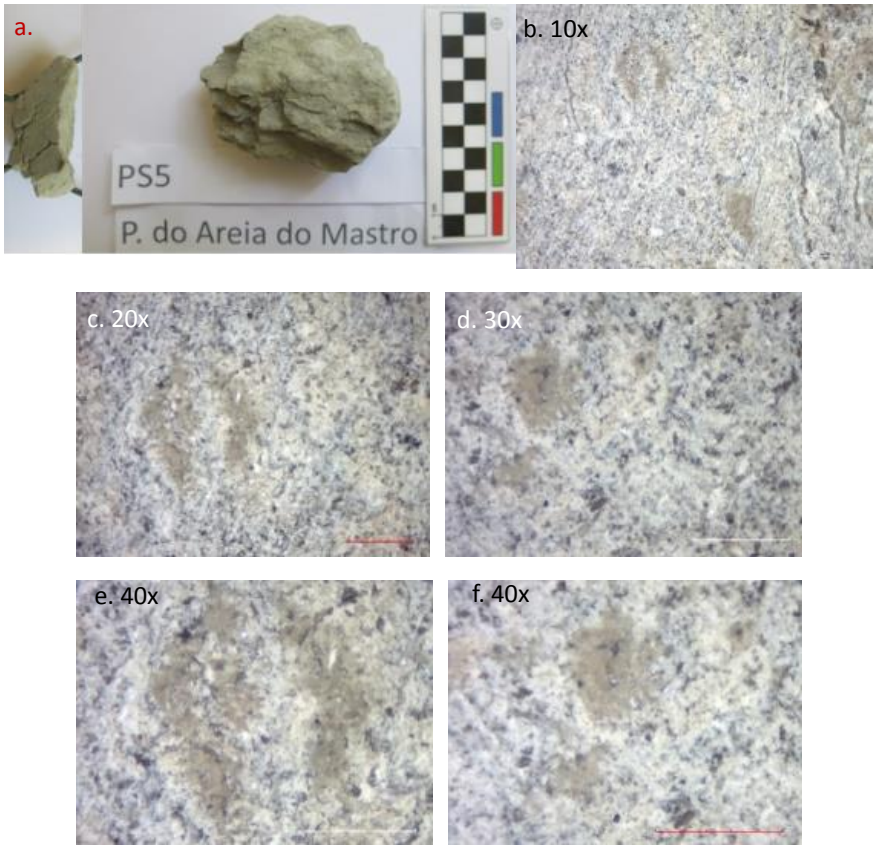


**Fig. 5.2.1. 4, Macroscopic (a) and microscopic (b to f, labeled with the magnification) photos of the sample PS5.**

Sample PS3 (Fig. 5.2.1.5a) macroscopically appears gray celadon in color. The color is slightly heterogeneous; the surface of the sample is rough to the touch and very resistant. This rock is very heavy and seems to have high density. The microscopic observations (Figure 5.1.1.5b to d) of the sample PS3 show that its main fraction is composed by carbonate mud, composed of very fine carbonate minerals. , A few quarts minerals are regularly distributed with the size mostly slightly smaller or equaled to 0,2 mm. Very few black irregular shaped particles of organic matter are also randomly located on the surface. The grain sizes of the particles in the sample PS3 depict that it belongs to a limestone with a sandy fraction in it.

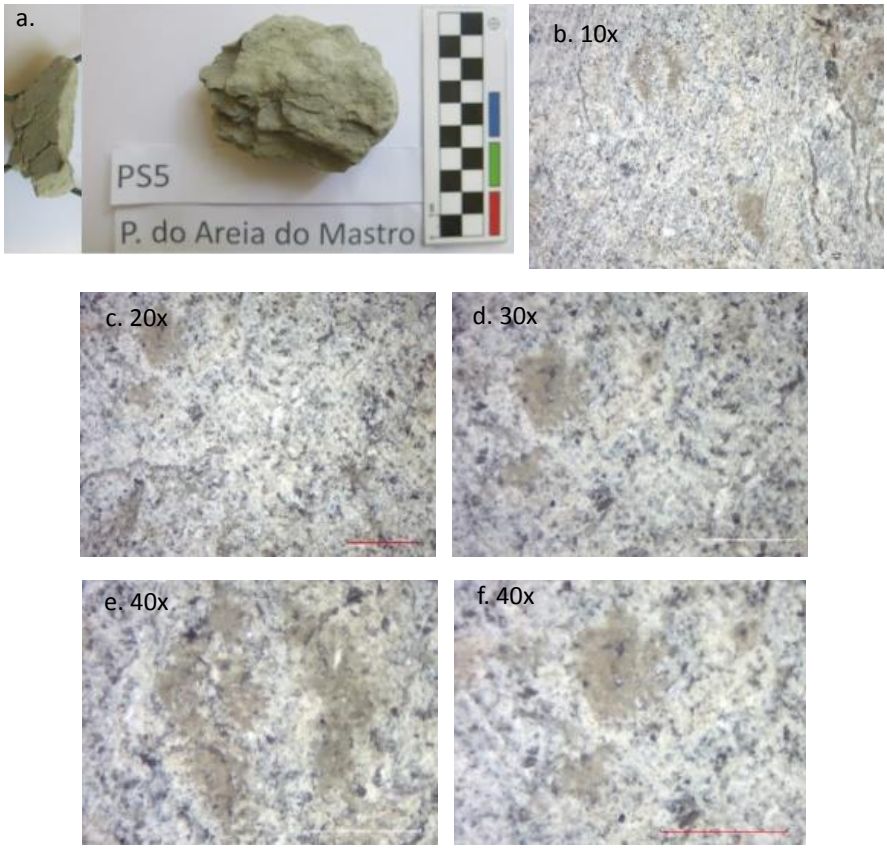


**Fig. 5.2.1. 5, Macroscopic (a) and microscopic (b to g, labeled with the magnification) photos of the sample PS3.**

Sample PS2 (Fig. 5.2.1.6a) macroscopically appears gray celadon and a little light khaki in color. The color is heterogeneous; the surface of the sample is dusty to the touch and very resistant. It is muddy, when mixed with or touched by water. The microscopic observations (Figure 5.2.1.6b to f) of the sample PS2 show that few milky beige feldspars and white quartz minerals with the size equaled to 1,0-1,5 mm immersed in a very lightly beige binders with very tiny size which is too small to be determined by scale bar (much smaller than 0,02 mm). The grain sizes of the particles in the sample PS2 depict that it belongs to mudstone with medium and fine sand.

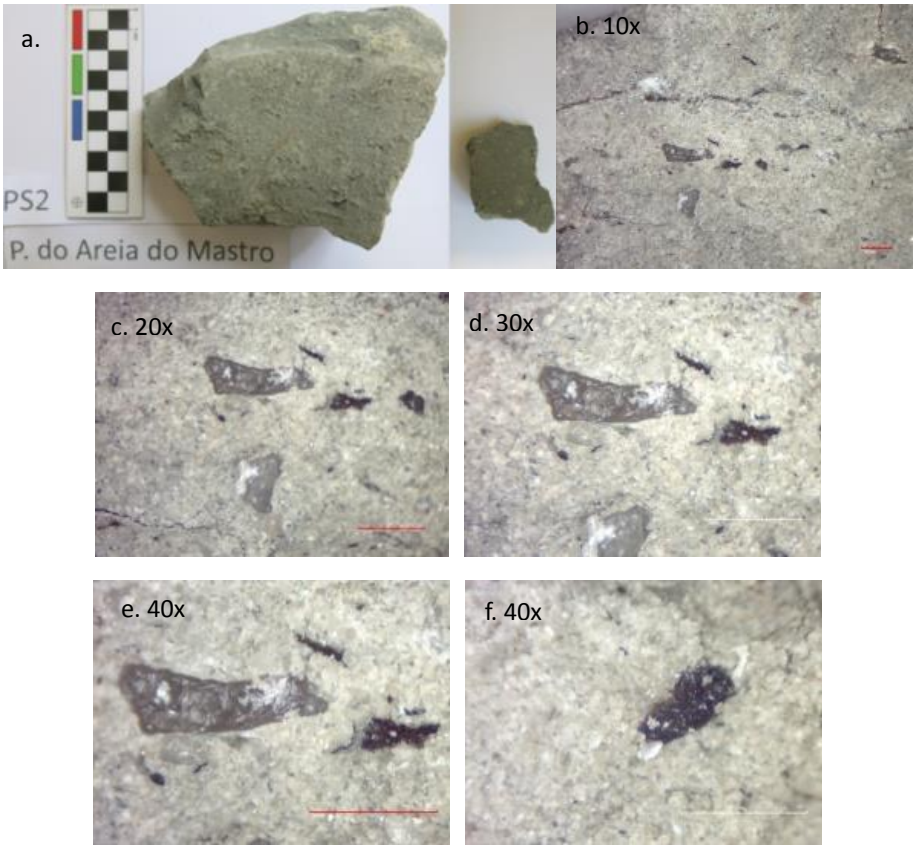


**Fig. 5.2.1. 6, Macroscopic (a) and microscopic (b to f, labeled with the magnification) photos of the sample PS2.**

Sample PS1 (Fig. 5.2.1.7a) macroscopically appears dark yellow-light green in color. The color is not homogeneous; the surface of the sample is sandy to the touch and quite resistant. The microscopic observations (Figure 5.2.1.7b to f) of the sample PS1 show that there are black and white minerals, quartz and feldspars, with the size roughly equaled to 0,6 mm on the sample's surface. The shining white particles of carbonates with the size smaller than 0,2 mm seem to be the binders filled between the 0,6 mm blocks. The grain sizes of the particles in the sample PS1 depict that it belongs to sandstone mainly consisting of medium and fine sand with a muddy fraction.

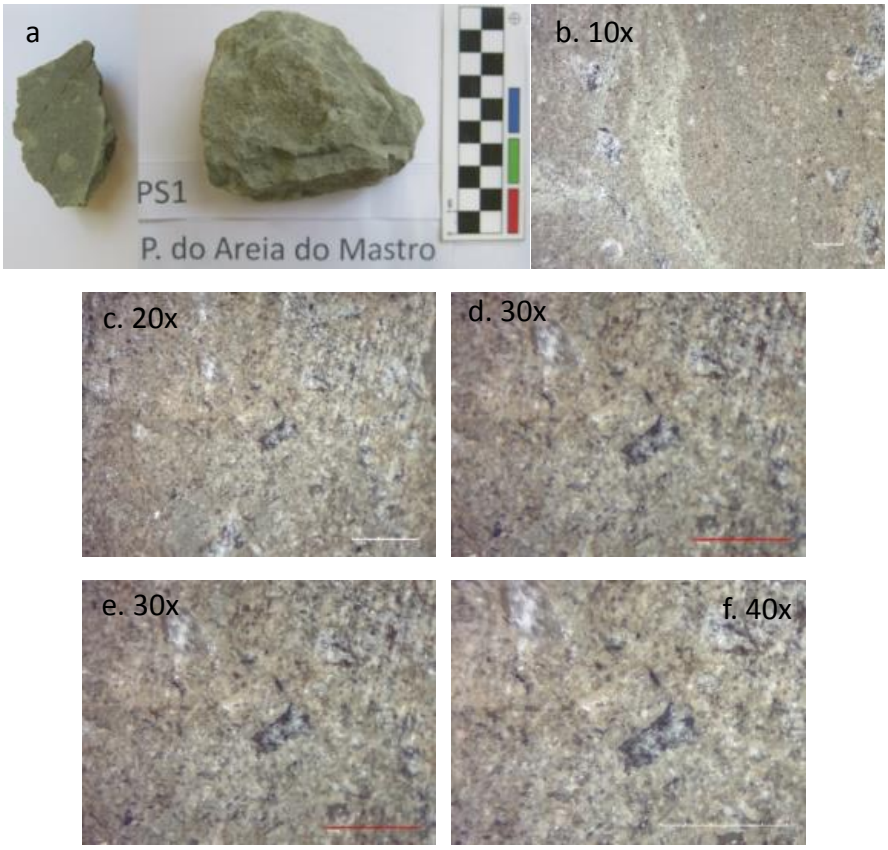


**Fig. 5.2.1. 7, Macroscopic (a) and microscopic (b to f, labeled with the magnification) photos of the sample PS1.**

### V.2.2 The samples of the Boca do Chapim site

The eleven samples (no. 1 to 11) of the Boca do Chapim site belong to the PS Form. (sample no. 3 to 11) and Areia do Mastro formation (AM Form.; sample no. 1 and 2 collected from this formation) and the stratum where they were collected are pointed out in the figure 5.2.2.1. According to Aillud (2001), Figueiredo et al. (2022b) and Cunha's unpublished data, the PS Form in this site along the same coastline north of the Espichel Cape consist of majorly silty gray marl or mud depositions with some grey carbonate silts and lenses of fine, ribbon, shaped, clastic sand; the AM Form is majorly composed of bluish-grey micritie clay-limestones and sandy (quartz-rich) micrite limestone. Compared to the description of the mentioned publications in this paragraph, the samples' photos for macroscopic and microscopic observations is shown in the paragraphs below in the order from the top layer to the bottom one–

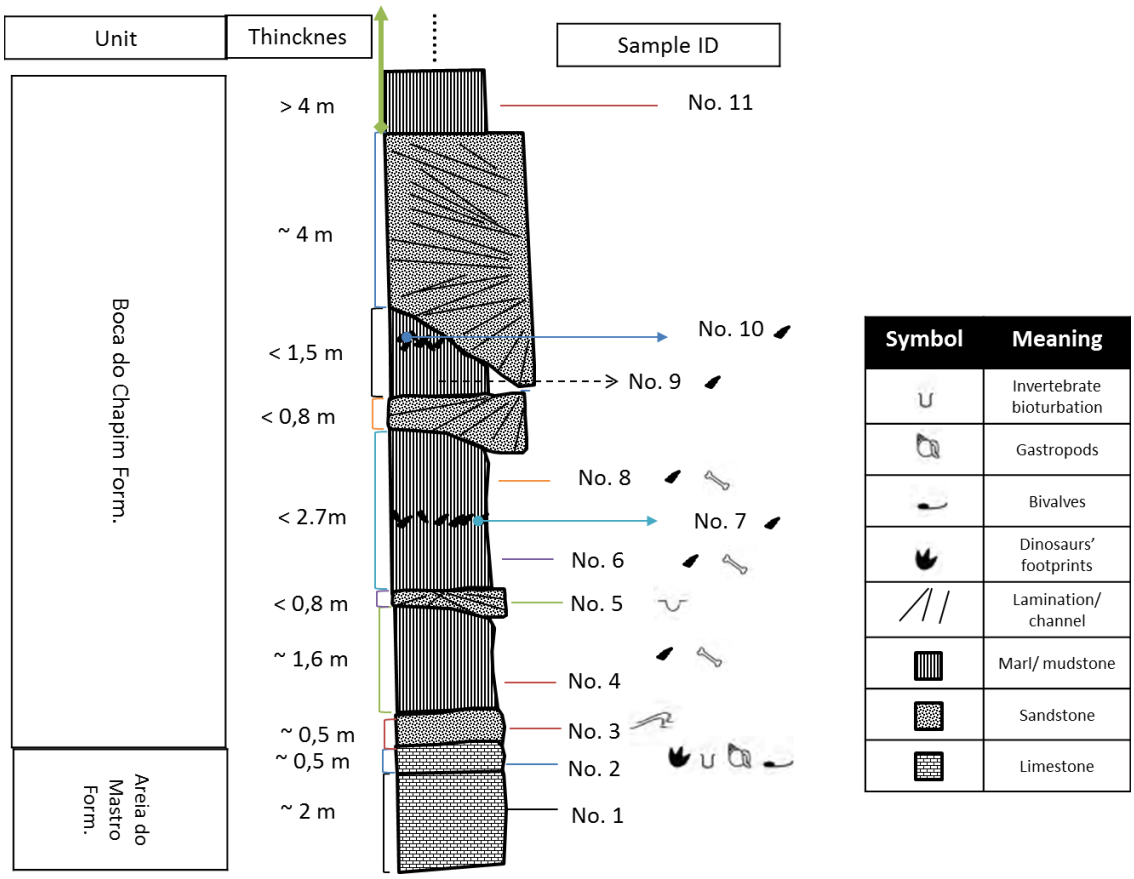


Fig. 5.2.2. 1, The sketched stratigraphic section of the Boca do Chapim site, with the labels to show the samples' collected stratum. (This sketch was drawn by the author and based on the unpublished data of Cunha's unpublished data and the work of Figueiredo et al. in 2022b)

Sample no. 11 (Fig. 5.2.2.2a) macroscopically appears gray celadon in color with a few dark red spots. The color is slightly heterogeneous; the surface of the sample is dusty to the touch and not resistant. It is muddy, when mixed with or touched by water. The microscopic observations (Figure 5.2.2.2b to f) of the sample no. 11 show that it was majorly full of beige particles with the size much smaller than 0,04 mm, and a few milky white irregular shaped minerals and black matters with the size roughly equaled to 0,2 mm and 0,1 mm respectively are distributed on the surface. The grain sizes of the particles in the sample no. 11 depict that it belongs to mudstone with a fraction of fine sand.

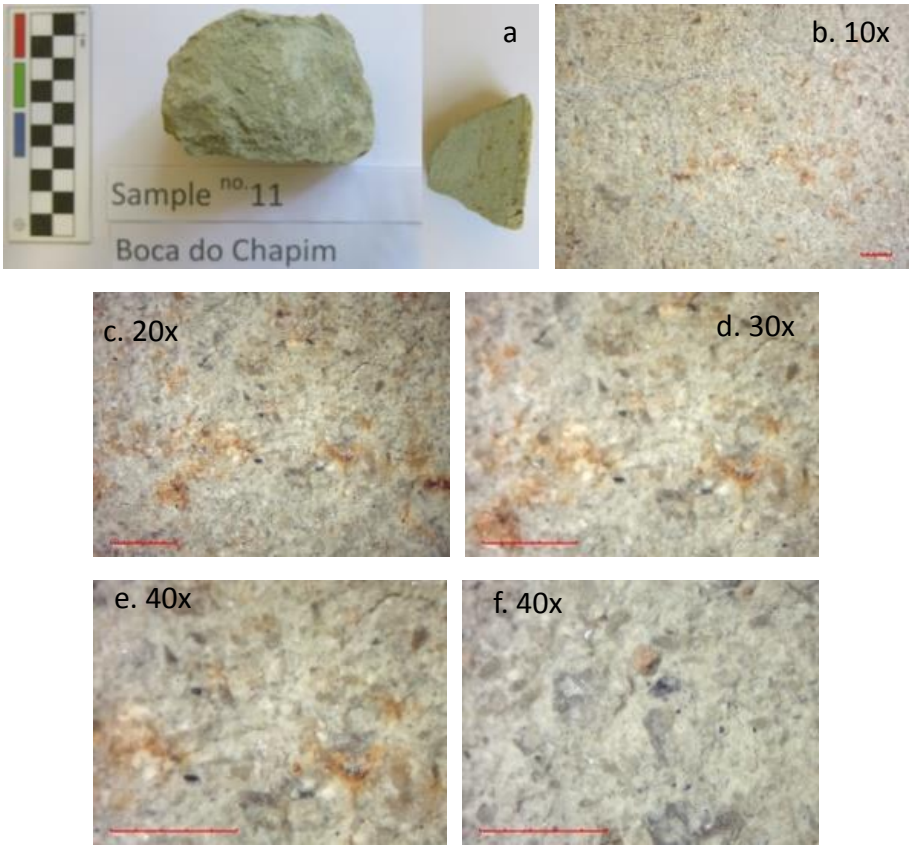


Fig. 5.2.2. 2, Macroscopic (a) and microscopic (b to f, labeled with the magnification) photos of the sample no. 11.

Sample no. 10 (Fig. 5.2.2.3a) macroscopically appears black in color and covered by few yellow powders. The color is very homogeneous, if the yellow powders are removed; the surface of the sample is sandy to the touch and not resistant. This sample's black and yellow color will stain the observer finger, if the observer touches it. The microscopic observations (Figure 5.2.2.3b to h) of the sample no. 10 show that the sample has a black surface covered by yellow, brown and shining white particles with the size around 0,02-0,05 mm. Very few shining white minerals with the size equaled to 0,8 mm are also embedded on the surface. According to Cunha's unpublished data and Figueiredo's work (2022b), this sample was collected from the sedimentary environment surrounded by significant mudstone and lagunal animals' fossils. Considering the grain sizes of the particles in this sample, the sedimentary conditions of it and the stratigraphic information in Figueiredo's work (2022b), this sample is lignite with few coarse mineral crystalline and numerous fine slits; furthermore, the yellow powders outside this sample is composed by sulfur minerals and very thin gypsum minerals.

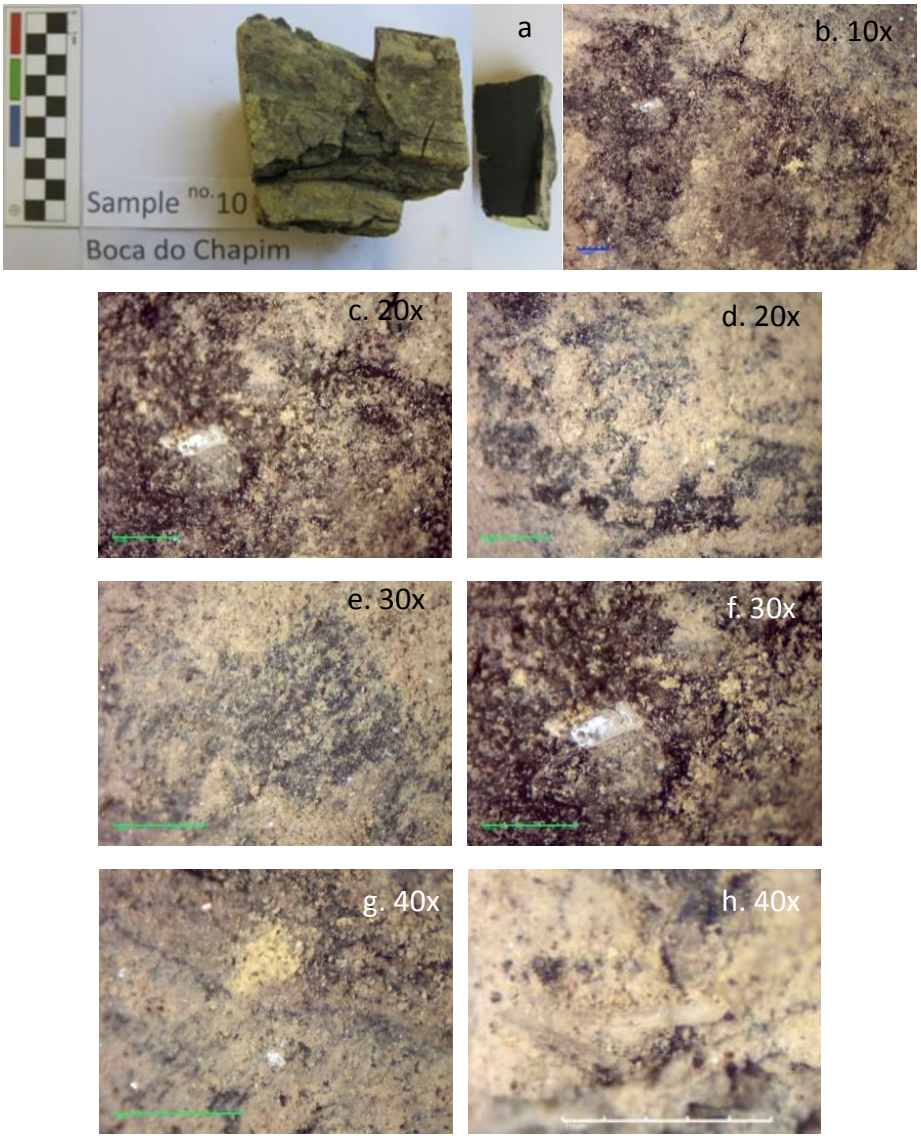


**Fig. 5.2.2. 3, Macroscopic (a) and microscopic (b to h, labeled with the magnification) photos of the sample no. 10.**

Sample no. 9 (Fig. 5.2.2.4a) macroscopically appears majorly gray celadon with a little light khaki in color. The color is heterogeneous; the surface of the sample is dusty to the touch and not resistant. It is muddy, when mixed with or touched by water. The microscopic observations (Figure 5.2.2.4b to f) of the sample no. 9 show that numerous milky white and gray irregular shaped minerals with the size equaled to 0,05-0,1 mm are surrounded by the brown binders with the size much smaller than 0,02 mm. A few black matters with the size around 0,2 mm are also embedded on the surface. The grain sizes of the particles in the sample no. 9 depict that it belongs to mudstone with a fraction of fine sand.

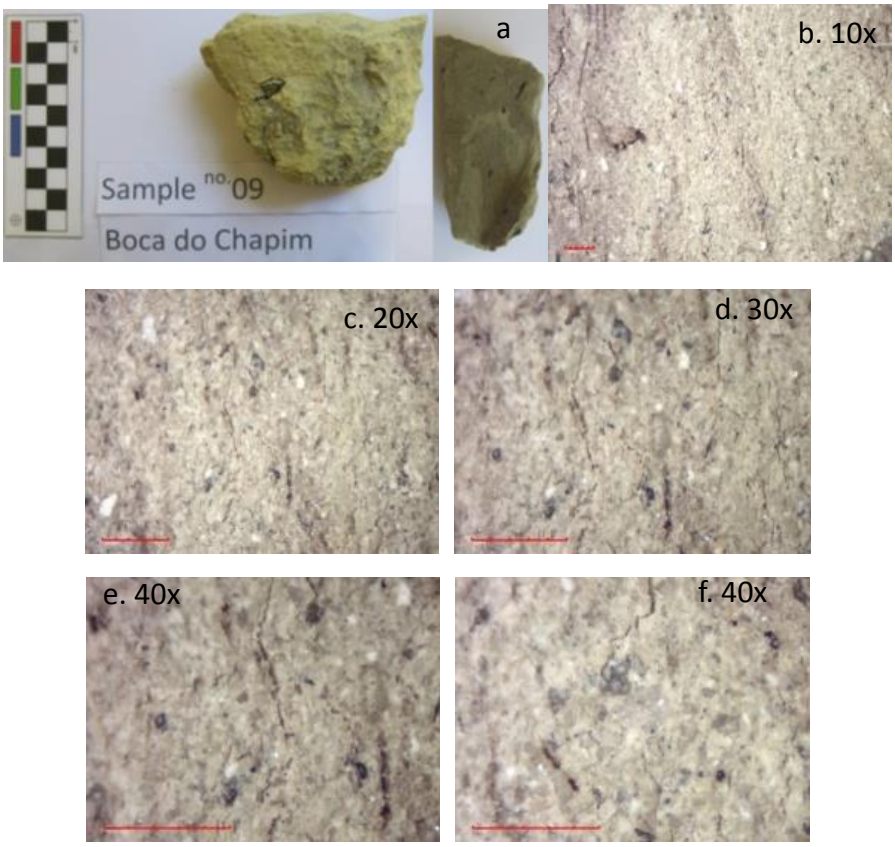


Fig. 5.2.2. 4, Macroscopic (a) and microscopic (b to f, labeled with the magnification) photos of the sample no. 9.

Sample no. 8 (Fig. 5.2.2.5a) macroscopically appears gray celadon with a little yellow and reddish brown in color. The color is heterogeneous; the surface of the sample is dusty to the touch and not resistant. It is muddy, when mixed with or touched by water. The microscopic observations (Figure 5.2.2.5b to f) of the sample no. 8 show that numerous irregularly shaped milky gray and black matters with the size around 0,2-0,1 mm are surrounded by light khaki binders with the size much smaller than 0,02 mm on it. Few groups of shining white spots with the size about 0,02 mm are also distributed on the surface. The grain sizes of the particles in the sample no. 8 depict that it belongs to mudstone with a fraction of fine sand.

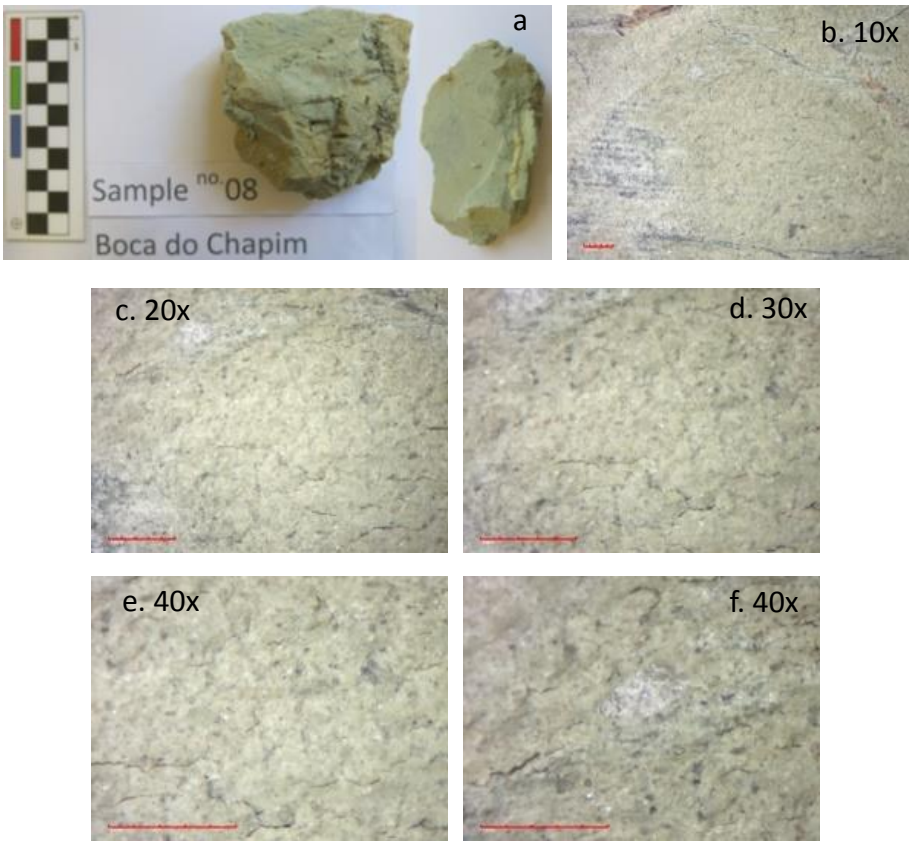


**Fig. 5.2.2. 5, Macroscopic (a) and microscopic (b to f, labeled with the magnification) photos of the sample no. 8.**

Sample no. 7 (Fig. 5.2.2.6a) has two parts. One part macroscopically appears black in color and is covered by several yellow dusts; the other macroscopically appears the milky gray in color and is also covered by several yellow dusts. The colors of both parts are homogeneous, if the yellow dusts are removed. The surface of the sample's black part is crispy to the touch and weakly resistant; that of the milky gray part is hard. The microscopic observations (Figure 5.2.2.6b to j) of the black part of the sample no. 7 show that its black surface is covered by numerous yellow, beige, white and crystal-like shining particles with the size around 0,02 mm. A few 0,04 mm-large shining crystal-like matters are also embedded on the surface. The microscopic observations (Figure 5.2.2.6k to p) of the sample no. 7 show that its milky gray mineral-like surface is covered by black, yellowish brown, and red particle with the size approximately equaled to 0,04 mm. According to Cunha's unpublished data and Figueiredo's work (2022b), this sample was collected from the sedimentary environment surrounded by significant mudstone and lagunal animals' fossils. Considering the grain sizes of the particles in this sample, the sedimentary conditions of it and the stratigraphic information in Figueiredo's work (2022b), this sample may be lignite few medium slits, and the milky gray one is the sedimentary rock mainly consisting of gypsum with few medium slits. Furthermore, the yellow powders outside this sample might be mixture matters of sulfur and gypsum minerals. The chemical composition of this sample and dusts on it should be carried out by the punctual analysis, such as the SEM-EDS and Raman spectrometer.


a
Sample no. 07
Boca do Chapim

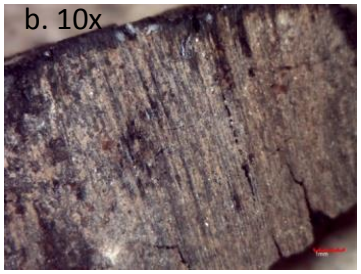
b. 10x

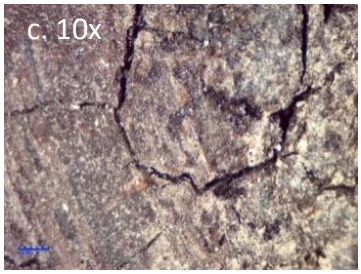
c. 10x

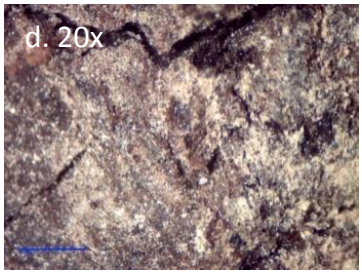
d. 20x


e. 20x

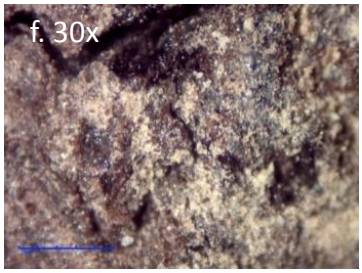
f. 30x

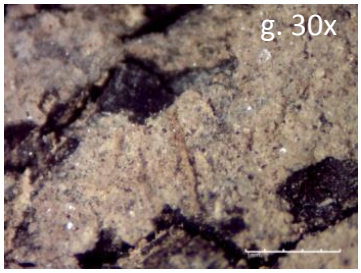
g. 30x

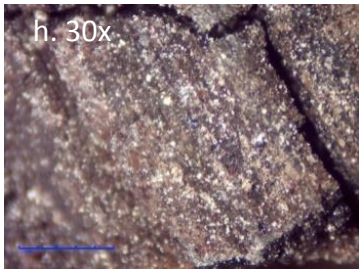
h. 30x

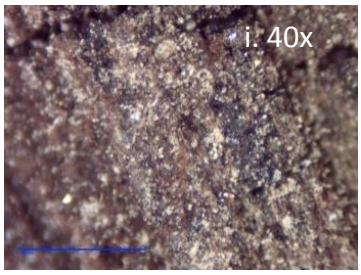
i. 40x

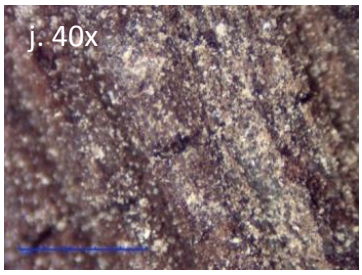
j. 40x

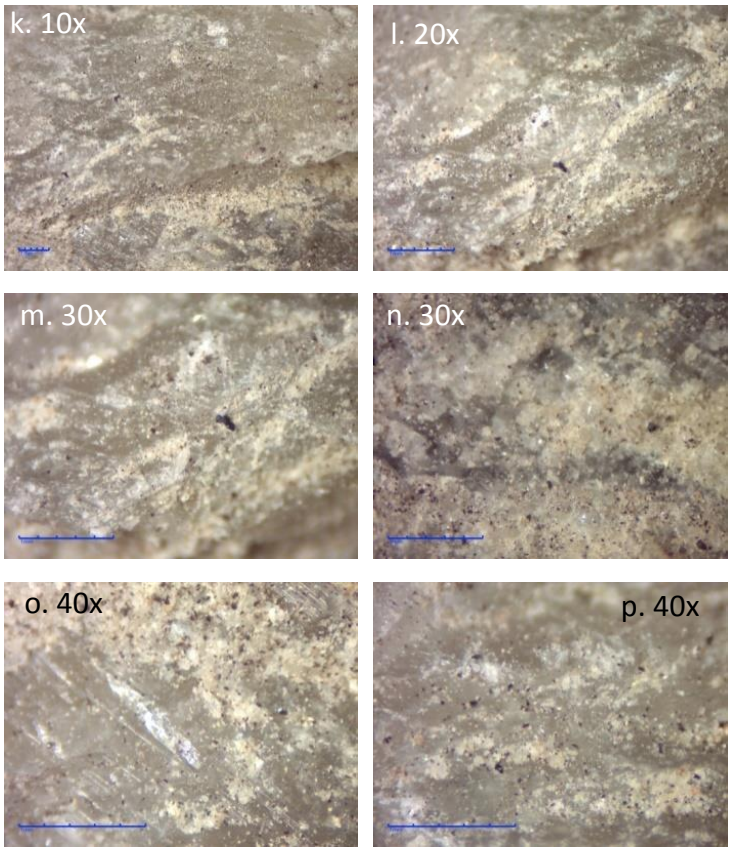


Fig. 5.2.2. 6, Macroscopic (a) and microscopic (lignite/ black one in the previous page – b to j, and beige one – k to p, all labeled with the magnification) photos of the sample no. 7.

Sample no. 6 (Fig. 5.2.2.7a) macroscopically appears gray celadon in color and is covered by several yellow dusts. The color is not very homogeneous; the surface of the sample is dusty to the touch and not resistant. It is muddy, when mixed with or touched by water. The microscopic observations (Figure 5.2.2.7b to f) of the sample no. 6 show that a few milky beige, black, brightly shining white and dark red irregularly shaped particles with the size around 0,08-0,2 mm is surrounded by gray celadon binders with the size much smaller than 0,02 mm. The grain sizes of the particles in the sample no. 6 depict that it belongs to mudstone with a fraction of fine sand.

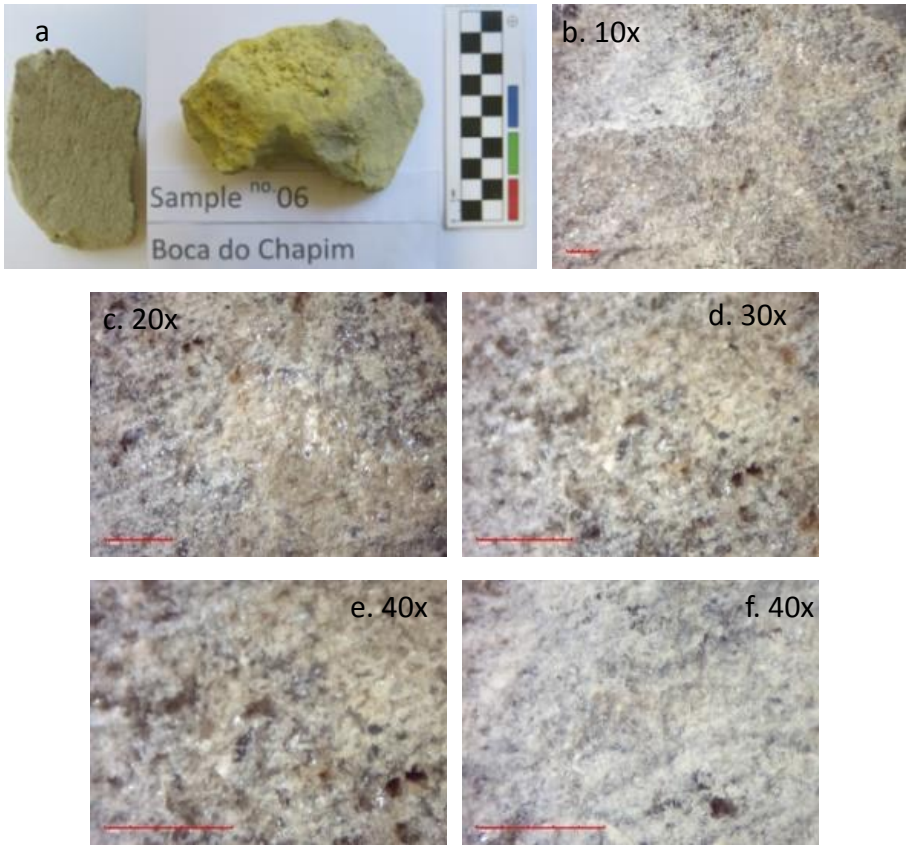


**Fig. 5.2.2. 7, Macroscopic (a) and microscopic (b to f, labeled with the magnification) photos of the sample no. 6.**

Sample no. 5 (Fig. 5.2.2.8a) macroscopically appears gray celadon in color with several red and black spots. The color is not very homogeneous; the surface of the sample is sandy to the touch and very resistant. The microscopic observations (Figure 5.2.2.8b to f) of the sample no. 5 show that it is characterized by a sandy fraction with the presence of fractures with calcite recrystallization. The sandy fraction is in part composed by carbonates and in part composed by terrigenous components. The grain sizes of the particles in the sample no. 5 depict that it belongs to sandstone consisting mainly of medium and fine sand.

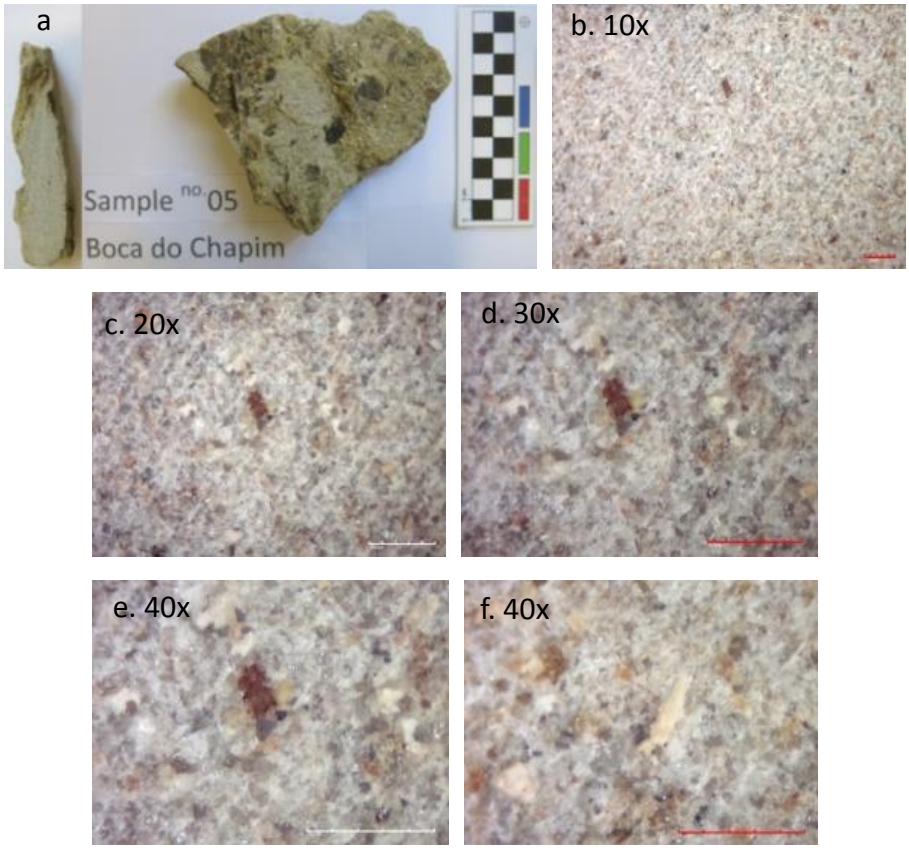


**Fig. 5.2.2. 8, Macroscopic (a) and microscopic (b to f, labeled with the magnification) photos of the sample no. 5.**

Sample no. 4 (Fig. 5.2.2.9a) macroscopically appears gray celadon in color and is covered by numerous yellow dusts. The color is heterogeneous; the surface of the sample is dusty to the touch and not resistant. It is muddy, when mixed with or touched by water. The microscopic observations (Figure 5.2.2.9b to f) of the sample no. 4 show that numerous 0,1-0,2 mm-large milky gray minerals and roughly 0,3 mm-large black sediments with white or red spots are surrounded by significant 0,02 mm-large (or smaller) white or gray celadon binders. The grain sizes of the particles in the sample no. 4 depict that it belongs to mudstone with a fraction of fine sand.

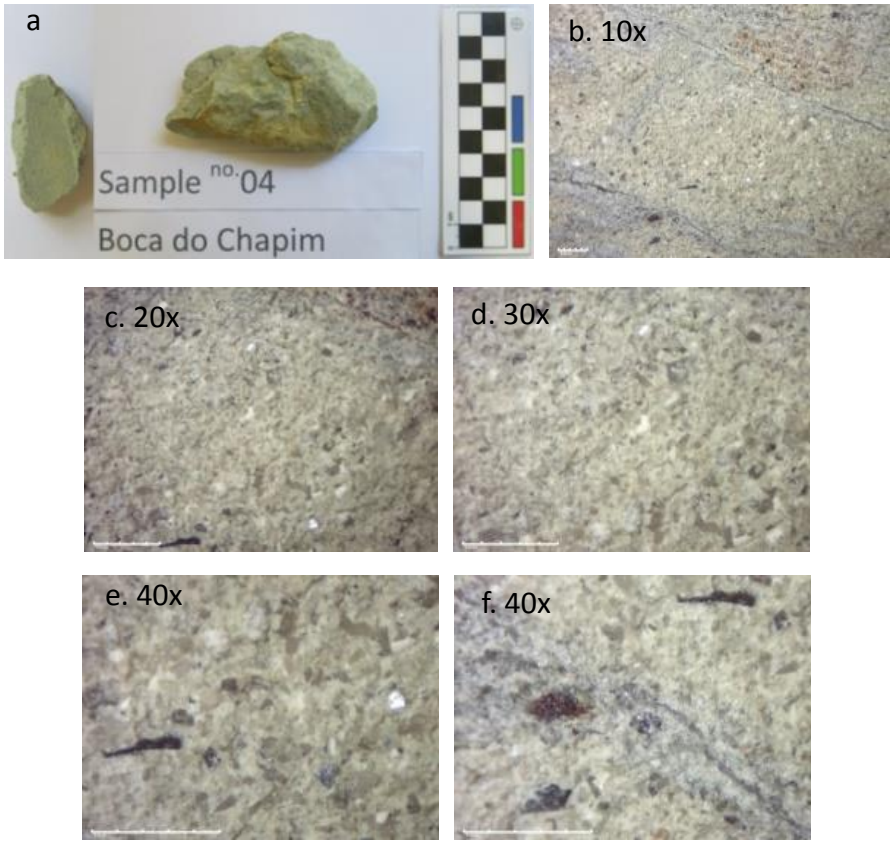


Fig. 5.2.2. 9, Macroscopic (a) and microscopic (b to f, labeled with the magnification) photo of the sample no. 4.

Sample no. 3 (Fig. 5.2.2.10a) macroscopically appears gray celadon in color with few black, yellow and reddish brown spots. The color is not very homogeneous; the surface of the sample is sandy to the touch and very resistant. The microscopic observations (Figure 5.2.2.10b to f) of the sample no. 3 show that several 0,2-1,0 mm-large reddish brown, black and gray irregularly shaped particles of organic matters in white, gray celadon and crystal-like shining binders with the size much smaller than 0,02 mm. The grain sizes of the particles in the sample no. 3 depict that it belongs to fine sandstone mainly carbonates in composition with a silty fraction.

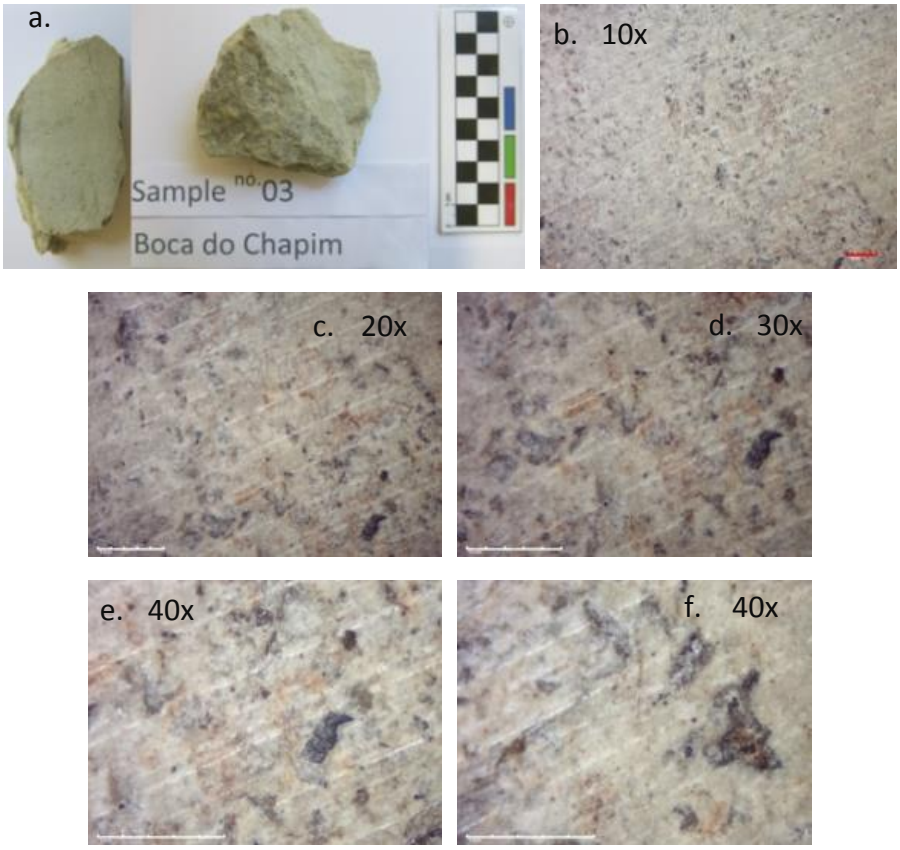


Fig. 5.2.2. 10, Macroscopic (a) and microscopic (b to f, labeled with the magnification) photos of the sample no. 3.

Sample no. 2 (Fig. 5.2.2.11a) macroscopically appears khaki in color with many reddish brown spots. The color is heterogeneous; the surface of the sample is sandy to the touch and very resistant. The microscopic observations (Figure 5.2.2.11b to f) of the sample no. 2 show that significant 0,1-0,16 mm-large milky gray minerals and some black irregularly shaped particles are filled with a few bright khaki and white carbonate binders with the size around 0,02 mm on the surface. Very few crystal-like shining particles with the size about 0,2 mm are also embedded on it. The grain sizes of the particles in the sample no. 2 depict that it belongs to carbonate siltstone consisting of mainly specifically mineral with fine sand.

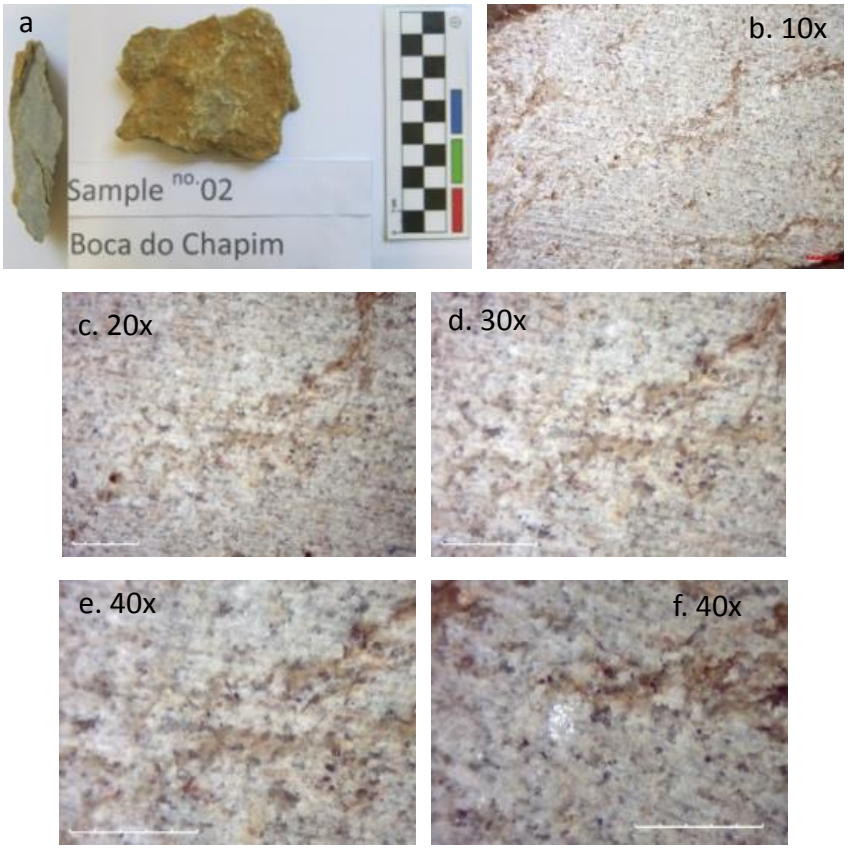


**Fig. 5.2.2. 11, Macroscopic (a) and microscopic (b to f, labeled with the magnification) photos of the sample no. 2.**

Sample no. 1 (Fig. 5.2.2.12a) macroscopically appears gray celadon in color (but whiter than the sample no. 2) with reddish brown and black spots. The color is heterogeneous; the surface of the sample is sandy to the touch and very resistant. The microscopic observations (Figure 5.2.2.12b to f) of the sample no. 1 show that majorly 0,1 mm-large milky gray, bright brown and white particles are located on the surface. Some roughly 0,02 mm-large black spots of organic matter are covered on some part of the surface. Very few 0,3 mm-large crystal-like matters are also embedded on it. The grain sizes of the particles in the sample no. 1 depict that it belongs to very fine carbonate sandstone consisting of mainly specifically fine-sandy mineral with a small fraction of silt.

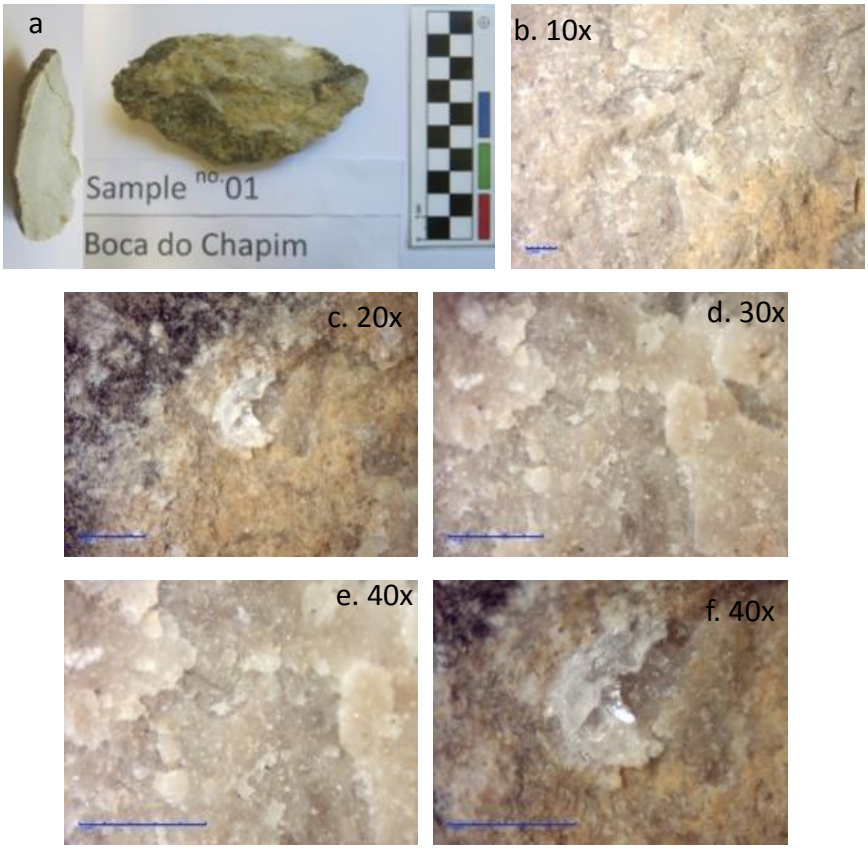


**Fig. 5.2.2 12, Macroscopic (a) and microscopic (b to f, labeled with the magnification) photos of the sample no.1.**

After the samples were roughly classified by the macroscopic and microscopic observations, the result of the chemical analysis in the sections V.3 to V.5 would depict to do the further identification for the more accurate classifications of sedimentary rocks for the samples.

## V.3 The calcimetric, total carbon content and L.O.I. analysis

### V.3.1 The samples from the Praia do Areia do Mastro site

The geochemical analysis for the quantity of the organic and inorganic carbon content, which contains the calcimetric, total carbon content and L.O.I. analysis at 500℃ and 1000℃, were carried out via following the methods described in the Chapter IV. The calcimetric, L.O.I analysis results of the samples were depicted in table 5.3.1.1 and 5.3.1.2, respectively. The data, which includes in the calcimetric, L.O.I and total carbon content (TC) analysis for the comparison of the organic and inorganic carbon content in the each sample, are shown in the table 5.3.1.3 and the diagram 5.3.1.1.

| Sample ID | $CO_2$ Percentage change in 60 s (/ %) | $CO_2$ Percentage change in 180 s (/ %) | $CO_2$ Percentage change in 900 s (/ %) |
|---|---|---|---|
| PS8 | 0 | 0 | 0 |
| PS7 | 13 | 13 | 13 |
| PS5 | 22 | 22 | 22 |
| PS3 | 54 | 54 | 54 |
| PS2 | 2 | 2 | 2 |
| PS1 | 4 | 11 | 18 |

Table 5.3.1. 1, The table depicts the percentage change of carbon dioxide in the calcimentric analysis in different time of the samples from the Praia do Areia do Mastro site's different strata

| Sample ID | L.O.I 500 (/ %) | L.O.I 1000 (/ %) | L.O.I 500 – L.O.I 1000 (/ %) |
|---|---|---|---|
| PS8 | 3,39 | 5,35 | 1,96 |
| PS7 | 2,28 | 9,59 | 7,32 |
| PS5 | 3,22 | 13,39 | 10,17 |
| PS3 | 2,63 | 25,56 | 22,92 |
| PS2 | 3,71 | 6,28 | 2,57 |
| PS1 | 4,24 | 13,04 | 8,80 |

Table 5.3.1. 2, The table depicts the percentage of volatile contents of the samples from the Praia do Areia do Mastro site's different strata after calcination at 500℃ (L.O.I 500), and 1000 ℃ (L.O.I 1000), and the difference of these two values (L.O.I 500 – L.O.I 1000).

| Sample ID | L.O.I. 500/ % | L.O.I. 1000/ % | Calcimetric 900s/ % | TC/ % |
|---|---|---|---|---|
| PS8 | 3,39 | 5,35 | 0 | 0,59 |
| PS7 | 2,28 | 9,59 | 13 | 2,17 |
| PS5 | 3,22 | 13,39 | 22 | 2,79 |
| PS3 | 2,63 | 25,56 | 54 | 6,22 |
| PS2 | 3,71 | 6,28 | 2 | 0,4 |
| PS1 | 4,24 | 13,04 | 18 | 2,64 |

Table 5.3.1. 3, The table depicts the Praia do Areia do Mastro site samples' organic and inorganic carbon content data, which includes in the L.O.I. 500, L.O.I. 1000, calcimetric analysis for 900 s and total carbon content percentage (TC).

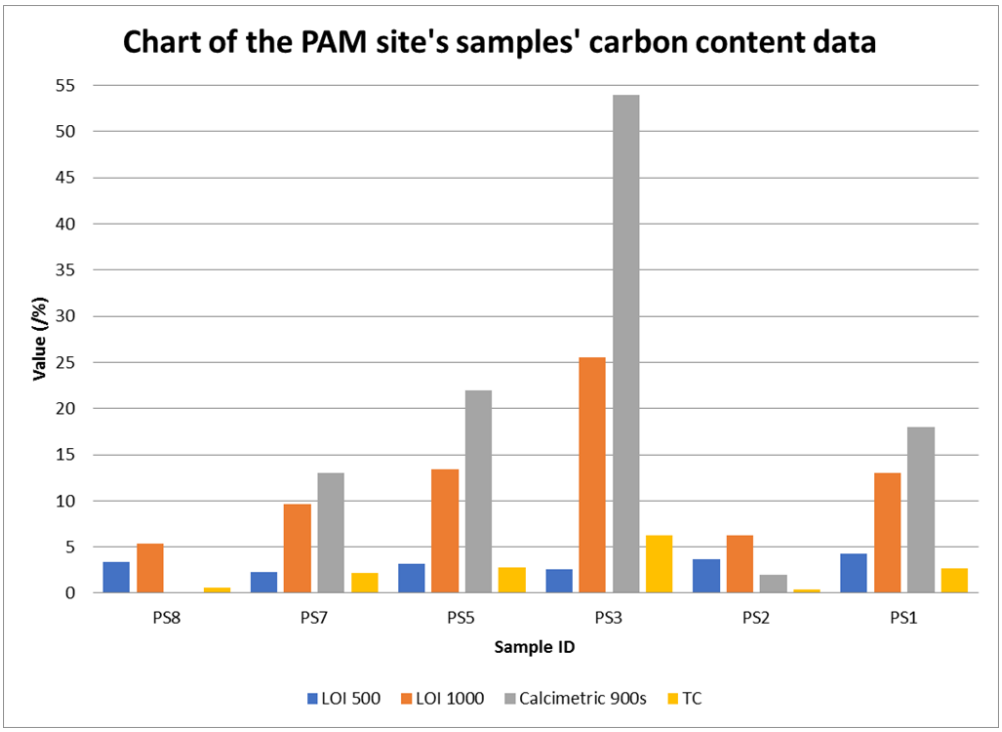


Diagram 5.3.1. 1, The bar chart illustrates the Praia do Areia do Mastro site samples' organic and inorganic carbon content data, which includes in the L.O.I. 500, L.O.I. 1000, calcimetric analysis for 900 s and TC percentage.

For the sample PS8, the result of the calcimetric analysis shows there is no $CO_2$ gas produced during the reaction of this sample and HCl for 900 s; the result of the L.O.I. analysis indicates there were 3,39% and 5,35% of the sample's weight loss after the calcination at 500℃ and 1000℃, respectively. The TC percentage of this sample is also only 0.59%. Combined to the macroscopic and microscopic observation result of this sample, the data represent that the sample is mainly composed by silicate and we can confirm that it is a silica-based mudstone with a fraction of fine quartz sand.

For the sample PS7, the result of the calcimetric analysis shows there is 13% of the $CO_2$ gas produced during the reaction of this sample and HCl for 900 s; the result of the L.O.I. analysis indicates there were 2,28% and 9,59% of the sample's weight loss after the calcination at 500℃ and 1000℃, respectively. The TC percentage of this sample is 2,17%. Combined to the macroscopic and microscopic observation result of this sample, it is possible to say that it is a silicate/ silica-based sandstone with a few organic and calcium carbonate-based minerals, typical of a polygenic limestone with a silty terrigenous fraction.

For the sample PS5, the result of the calcimetric analysis shows there is 22% of the $CO_2$ gas produced during the reaction of this sample and HCl for 900 s; the result of the L.O.I. analysis indicates there were 3,22% and 13,39% of the sample's weight loss after the calcination at 500℃ and 1000℃, respectively. The TC percentage of this sample is 2,79%. Combined to the macroscopic and microscopic observation result of this sample, it is a mudstone-based rock (marl) with both carbonate component (limestone) and silty terrigenous fraction.

For the sample PS3, the result of the calcimetric analysis shows there is 54% of the $CO_2$ gas produced during the reaction of this sample and HCl for 900 s; the result of the L.O.I. analysis indicates there were 2,63% and 25,56% of the sample's weight loss after the calcination at 500℃ and 1000℃, respectively. The TC percentage of this sample is 6,22%. Combined to the macroscopic and microscopic observation result of this sample, it is a limestone with a quartz sandy fraction.

For the sample PS2, the result of the calcimetric analysis shows there is 2% of the $CO_2$ gas produced during the reaction of this sample and HCl for 900 s; the result of the L.O.I. analysis indicates there were 3,17% and 6,28% of the sample's weight loss after the calcination at 500℃ and 1000℃, respectively. The TC percentage of this sample is only 0,4%. Combined to the macroscopic and microscopic observation result of this sample, it is a silicate/ silica-based clay mudstone with few calcium carbonate medium and fine sand.

For the sample PS1, the result of the calcimetric analysis shows there is 4%, 11% and 18% of the $CO_2$ gas produced after the reaction of this sample and HCl for 60 s, 180s and 900 s, respectively; the result of the L.O.I. analysis indicates there were 4,24% and 13,04% of the sample's weight loss after the calcination at 500℃ and 1000℃, respectively. The TC percentage of this sample is 2,64%. Combined to the macroscopic and microscopic observation result of this sample, it is a sandstone mainly consisting of calcium carbonate and various carbonate medium and fine sand with a majorly quartz and few organic muddy fraction.

### V.3.2 The samples from the Boca do Chapim site

The geochemical analysis for the quantity of the organic and inorganic carbon content, which contains the calcimetric, total carbon content and L.O.I. analysis at 500℃ and 1000℃, were carried out via following the methods described in the Chapter IV. The calcimetric, L.O.I analysis results of the samples were depicted in table 5.3.2.1 and 5.3.2.2, respectively. The data, which includes in the calcimetric, L.O.I and total carbon content (TC) analysis for the comparison of the organic and inorganic carbon content in the each sample, are shown in the table 5.3.2.3 and the diagram 5.3.2.1.

| Sample ID | $CO_2$ Percentage change in 60 s (/ %) | $CO_2$ Percentage change in 180 s (/ %) | $CO_2$ Percentage change in 900 s (/ %) |
|---|---|---|---|
| Sample no. 11 | 0 | 0 | 0 |
| Sample no. 10 | 0 | 0 | 0 |
| Sample no. 9 | 0 | 0 | 0 |
| Sample no. 8 | 0 | 0 | 0 |
| Sample no. 7 | 0 | 0 | 0 |
| Sample no. 6 | 0 | 0 | 0 |
| Sample no. 5 | 30 | 30 | 30 |
| Sample no. 4 | 0 | 0 | 0 |
| Sample no. 3 | 84 | 84 | 84 |
| Sample no. 2 | 88 | 88 | 88 |
| Sample no. 1 | 93 | 93 | 93 |

Table 5.3.2. 1, The table depicts the percentage change of carbon dioxide in the calcimentric analysis in different time of the samples from the Boca do Chapim site

| Sample ID | L.O.I 500 (/ %) | L.O.I 1000 (/ %) | L.O.I 500 – L.O.I 1000 (/ %) |
|---|---|---|---|
| no. 11 | 3,43 | 5,12 | 1,69 |
| no. 10 | 93,55 | 94,36 | 0,81 |
| no. 9 | 6,04 | 8,35 | 2,31 |
| no. 8 | 4,12 | 6,29 | 2,17 |
| no. 7 | 81,20 | 83,66 | 2,45 |
| no. 6 | 4,76 | 6,13 | 1,38 |
| no. 5 | 1,40 | 14,24 | 12,84 |
| no. 4 | 3,18 | 4,46 | 1,28 |
| no. 3 | 2,15 | 35,75 | 33,60 |
| no. 2 | 1,50 | 39,67 | 38,17 |
| no. 1 | 1,35 | 41,24 | 39,89 |

Table 5.3.2. 2, The table depicts the loss percentage of volatile contents of the samples from the Boca do Chapim site after calcination at 500°C (L.O.I 500), and 1000°C (L.O.I 1000), and the difference of these two values (L.O.I 500 – L.O.I 1000).

| Sample ID | L.O.I. 500/ % | L.O.I. 1000/ % | Calcimetric 900s/ % | TC/ % |
|---|---|---|---|---|
| no. 11 | 3,43 | 5,12 | 0 | 0,04 |
| no. 10 | 93,55 | 94,36 | 0 | 55,3 |
| no. 9 | 6,04 | 8,35 | 0 | 0,63 |
| no. 8 | 4,12 | 6,29 | 0 | 0,06 |
| no. 7 | 81,20 | 83,66 | 0 | 42,44 |
| no. 6 | 4,76 | 6,13 | 0 | 0,20 |
| no. 5 | 1,40 | 14,24 | 30 | 3,55 |
| no. 4 | 3,18 | 4,46 | 0 | 0,07 |
| no. 3 | 2,15 | 35,75 | 84 | 9,58 |
| no. 2 | 1,50 | 39,67 | 88 | 10,85 |
| no. 1 | 1,35 | 41,24 | 93 | 11,15 |

Table 5.3.2. 3, The table depicts the Praia do Areia do Mastro site samples' organic and inorganic carbon content data, which includes in the L.O.I. 500, L.O.I. 1000, calcimetric analysis for 900 s and total carbon content percentage (TC).

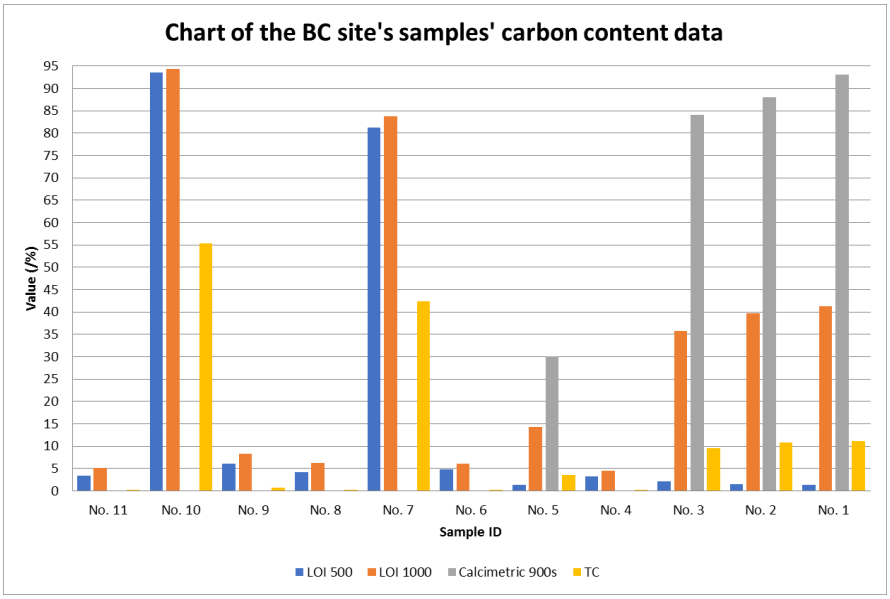


Diagram 5.3.2. 1, The bar chart illustrates the Boca do Chapim site samples' organic and inorganic carbon content data, which includes in the L.O.I. 500, L.O.I. 1000, calcimetric analysis for 900 s and TC percentage.

For the sample no. 11, the result of the calcimetric analysis shows there is no $CO_2$ gas produced during the reaction of this sample and HCl for 900 s; the result of the L.O.I. analysis indicates there were 3,43% and 5,12% of the sample's weight loss after the calcination at 500℃ and 1000℃, respectively. The TC percentage of this sample is 0,04%. Combined to the macroscopic and microscopic observation result of this sample, it is a silicate/ silica-based clay mudstone with a fraction of very few fine silica sand with organic components.

For the sample no. 10, the result of the calcimetric analysis shows there is no $CO_2$ gas produced during the reaction of this sample and HCl for 900 s; the result of the L.O.I. analysis indicates there were 93,55% and 94,36% of the sample's weight loss after the calcination at 500℃ and 1000℃, respectively. The TC percentage of this sample is 55,30%. Combined to the macroscopic and microscopic observation result of this sample, it is lignite with few coarse mineral crystalline and numerous fine slits. Furthermore, the yellow powders outside this sample may be composed by sulfur minerals and very thin gypsum minerals, and it should be further carried out by the punctual analysis, such as the SEM-EDS or Raman spectrometer.

For the sample no. 9, the result of the calcimetric analysis shows there is no $CO_2$ gas produced during the reaction of this sample and HCl for 900 s; the result of the L.O.I. analysis indicates there were 6,04% and 8,35% of the sample's weight loss after the calcination at 500℃ and 1000℃, respectively. The TC percentage of this sample is 0,63%. Combined to the macroscopic and microscopic observation result of this sample, it is a silicate/ silica-based clay mudstone with a fraction of very few fine silica sand with organic components.

For the sample no. 8, the result of the calcimetric analysis shows there is no $CO_2$ gas produced during the reaction of this sample and HCl for 900 s; the result of the L.O.I. analysis indicates there were 4,12% and 6,29% of the sample's weight loss after the calcination at 500℃ and 1000℃, respectively. The TC percentage of this sample is 0,06%. Combined to the macroscopic and microscopic observation result of this sample, it is a silicate/ silica-based clay mudstone with a fraction of very little organic fine silica sand with organic components.

For the black part of the sample no. 7, the result of the calcimetric analysis shows there is not the $CO_2$ gas produced during the reaction of this sample and HCl for 900 s; the result of the L.O.I. analysis indicates there were 81,20% and 83,66% of the sample's weight loss after the calcination at 500℃ and 1000℃, respectively. The TC percentage of this sample is 42,4%. Combined to the macroscopic and microscopic observation result of this sample, it is lignite with few coarse mineral crystalline and numerous fine slits, but the content of carbon is around 10% less than the sample no. 10. Furthermore, the yellow powders outside this sample may be composed by sulfur minerals and very thin gypsum minerals, which might be more than the sample no. 10 because the large gypsum minerals even can be seen in naked eye on the sample no. 7, but it should be further carried out by the punctual analysis, such as the SEM-EDS or Raman spectrometer.

For the sample no. 6, the result of the calcimetric analysis shows there is no $CO_2$ gas produced during the reaction of this sample and HCl for 900 s; the result of the L.O.I. analysis indicates there were 4,76% and 6,13% of the sample's weight loss after the

calcination at 500℃ and 1000℃, respectively. The TC percentage of this sample is 0,20%. Combined to the macroscopic and microscopic observation result of this sample, it is a silicate/ silica-based clay mudstone with a fraction of very little organic fine siliclastic sand.

For the sample no. 5, the result of the calcimetric analysis shows there is 30% of the $CO_2$ gas produced during the reaction of this sample and HCl for 900 s; the result of the L.O.I. analysis indicates there were 1,40% and 14,24% of the sample's weight loss after the calcination at 500℃ and 1000℃, respectively. The TC percentage of this sample is 3,55%. Combined to the macroscopic and microscopic observation result of this sample, it is sandstone consisting mainly of medium and fine calcium carbonate sand with a silty terrigenous very fine fraction.

For the sample no. 4, the result of the calcimetric analysis shows there is no $CO_2$ gas produced during the reaction of this sample and HCl for 900 s; the result of the L.O.I. analysis indicates there were 3,18% and 4,46% of the sample's weight loss after the calcination at 500℃ and 1000℃, respectively. The TC percentage of this sample is only 0,07%. Combined to the macroscopic and microscopic observation result of this sample, it is a silicate/ silica-based clay mudstone with a fraction of very little, fine and organic sand.

For the sample no. 3, the result of the calcimetric analysis shows there is 84% of the $CO_2$ gas produced during the reaction of this sample and HCl for 900 s; the result of the L.O.I. analysis indicates there were 2,15% and 35,75% of the sample's weight loss after the calcination at 500℃ and 1000℃, respectively. The TC percentage of this sample is 9,58%. Combined to the macroscopic and microscopic observation result of

this sample, it is fine calcium carbonate-based sandstone mainly carbonate in composition with a few silty fractions.

For the sample no. 2, the result of the calcimetric analysis shows there is 88% of the $CO_2$ gas produced during the reaction of this sample and HCl for 900 s; the result of the L.O.I. analysis indicates there were 1,50% and 39,67% of the sample's weight loss after the calcination at 500℃ and 1000℃, respectively. The TC percentage of this sample is 10,85%. Combined to the macroscopic and microscopic observation result of this sample, it is limestone with fine inorganic and organic sandy matters.

For the sample no. 1, the result of the calcimetric analysis shows there is 93% of the $CO_2$ gas produced during the reaction of this sample and HCl for 900 s; the result of the L.O.I. analysis indicates there were 1,35% and 41,24% of the sample's weight loss after the calcination at 500℃ and 1000℃, respectively. The TC percentage of this sample is 11,15%. Combined to the macroscopic and microscopic observation result of this sample, it is fine calcium carbonate sandy-limestone and a very small fraction of silt.

## V.4 The EA-IRMS analysis

### V.4.1 The samples of the Praia do Areia do Mastro site

The EA-IRMS analysis for the total carbon contents (TC) and $\delta^{13}C$ value of the Praia do Ariea do Mastro site are shown on the table 5.4.1.1, and the bar chart of this site's calcimetric, TC and $\delta^{13}C$ value is illustrated on the diagram 5.4.1.1. All the samples collected from this site are analyzed by the EA-IRMS instrumental for three times; because all the standard deviation (STD) of the $\delta^{13}C$ analysis result are less than 0,500 ‰, it is allowed to calculate the average value by using these $\delta^{13}C$ results for each sample.

| Sample ID | TC (/ %) | Avg. $\delta^{13}C$ (/ ‰) | STD (/ ‰) |
|---|---|---|---|
| PS8 | 0,59 | -19,077 | 0,184 |
| PS7 | 2,17 | -3,428 | 0,038 |
| PS5 | 2,79 | -1,009 | 0,014 |
| PS3 | 6,22 | -4,311 | 0,041 |
| PS2 | 0,40 | -13,303 | 0,038 |
| PS1 | 2,64 | -1,352 | 0,030 |

**Table 5.4.1. 1, The total carbon contents and $\delta^{13}C$ values of the samples from the Praia do Areia do Mastro site.**

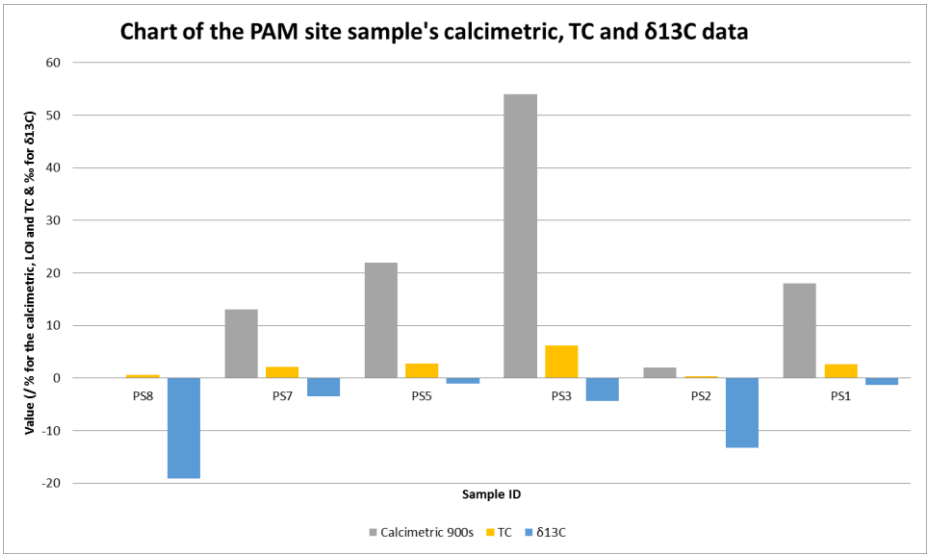


**Diagram 5.4.1. 1, The bar chart of the calcimetric analysis for 900 s and total carbon contents (TC), and $\delta^{13}C$ values of the samples from the Praia do Areia do Mastro site.**

In general, the sample PS5 has the highest $\delta^{13}C$ value (-1,009‰) and the sample PS8 has the lowest $\delta^{13}C$ value (-19,077‰). The samples with more calcium carbonate contents seem to generally have higher $\delta^{13}C$ value, but it is not totally correlative. In this section, the samples collected from the Praia do Areia do Mastro site would be classified as three groups, which are based on their geochemical compositions, to do the discussion and comparison of their $\delta^{13}C$ value –

- Sample with no calcium carbonate: The sample PS8
- Sample with calcium carbonate but almost no organic matter: The sample PS7, 5, 3 and 1
- Sample with a little calcium carbonate and organic matter: The sample PS2

For the group of the samples with no calcium carbonate, this kind of sample (only sample PS8) have very low $\delta^{13}C$ value (-19,077‰). Because there is no calcium carbonate and carbonates contents in it and only 0,59% of carbon content inside, based on the result of the TC and calcimetric analysis result, it may be hypothesized

that all of the carbon element in this sample is given by the organic compositions in it.

For the sample with calcium carbonate but almost no organic matter, the sample PS5 has the highest $\delta^{13}C$ value (-1,009‰) and the sample PS3 has the lowest $\delta^{13}C$ value (-4,311‰). The samples in this group all have high $\delta^{13}C$ value, compared to the other two groups. In these two samples two carbon sources can be identified carbonates contents and organic matters, which also contribute the $\delta^{13}C$ values of these samples.

For the sample with a little calcium carbonate and organic matter, the sample of this group (only the sample PS2) has very low $\delta^{13}C$ value (-13,303‰). The organic matters and calcium carbonate contents in this sample contributes its $\delta^{13}C$ value, although the total carbon content value (TC: 0,4%) and carbonates contents (calcimetric 900 s: 2%) of this sample is pretty low.

### V.4.2 The samples of the Boca do Chapim site

The EA-IRMS analysis for the total carbon contents (TC) and $\delta^{13}C$ value of the Boca do Chapim site are shown on the table 5.4.2.1, and the bar chart of this site's calcimetric, TC and $\delta^{13}C$ value is illustrated on the diagram 5.4.2.1. All the samples collected from this site are analyzed by the EA-IRMS instrumental for three times; because all the standard deviation (STD) of the $\delta^{13}C$ analysis result are less than 0,500 ‰, it is allowed to calculate the average value by using these $\delta^{13}C$ results for each sample.

| Sample ID | TC (/ %) | Avg. $\delta^{13}C$ (/ ‰) | STD (/ ‰) |
|---|---|---|---|
| no. 11 | 0,04 | -23,761 | 0,360 |
| no. 10 | 55,30 | -20,432 | 0,033 |
| no. 9 | 0,63 | -21,402 | 0,073 |
| no. 8 | 0,06 | -22,547 | 0,093 |
| no. 7 | 42,44 | -19,523 | 0,005 |
| no. 6 | 0,20 | -20,921 | 0,116 |
| no. 5 | 3,55 | -1,597 | 0,089 |
| no. 4 | 0,07 | -22,366 | 0,253 |
| no. 3 | 9,58 | -2,069 | 0,077 |
| no. 2 | 10,85 | -1,085 | 0,341 |
| no. 1 | 11,15 | -0,066 | 0,094 |

**Table 5.4.2. 1, The total carbon contents and $\delta^{13}C$ values of the samples from the Boca do Chapim site.**

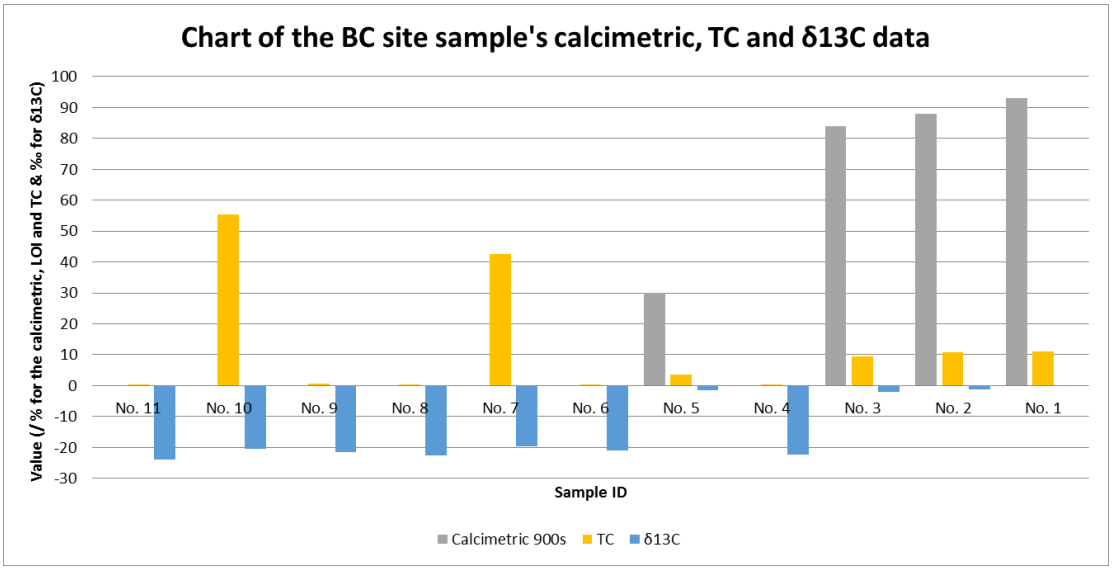


**Diagram 5.4.2. 1, The bar chart of the calcimetric analysis for 900 s and total carbon contents (TC), and $\delta^{13}C$ values of the samples from the Boca do Chapim site.**

In general, the sample no.1 has the highest $\delta^{13}C$ value (-0,066‰) and the sample no.11 has the lowest $\delta^{13}C$ value (-23,761‰). The samples with more calcium carbonate contents seem to have higher $\delta^{13}C$ value. In this section, the samples collected from the Boca do Chapim site would be classified as three groups, which are based on their grain size and geochemical compositions, to do the discussion and comparison of their $\delta^{13}C$ value –

- Mudstone: Samples no. 11, 9, 8, 6 and 4
- Lignite: Sample no. 10 and 7
- Limestone and sandstone with several calcium carbonate: Sample no.5, 3, 2 and 1

For the mudstone samples, these samples have very similar $\delta^{13}C$ values, which are around -24‰ to -20‰. All of these samples have no calcium carbonate, but have very little organic carbon matter. The $\delta^{13}C$ values of them seem correlated to their

total organic carbon contents, since in these five samples, the sample no.11 has lowest $\delta^{13}C$ value (-23,761‰) and highest TC value (0,04%), and the sample no.6 has highest $\delta^{13}C$ value (-20,921‰) and highest TC value (0,20%).

For the lignite samples, they both have very high TC contents (the sample no.10 has 55,30% and the sample no.7 has 42,44%), but they both have very low $\delta^{13}C$ values, which are -23,761‰ for the sample no.10 and -19,519‰.

For the samples of limestone and sandstone with several calcium carbonate, the sample no.1 has the highest $\delta^{13}C$ value (-0,066‰) and the sample no.3 has the lowest $\delta^{13}C$ value (-2.069‰). In the samples of this site, the ones with more calcium carbonate contents seem to have higher $\delta^{13}C$ value. However, in the samples of this group, the sample no.5, with only a half of calcium carbonate contents of the sample no.3 (its $\delta^{13}C$ is -1,085‰), has more $\delta^{13}C$ value than the sample no.3, whose $\delta^{13}C$ value is the lowest.

## V.5 The ICP-MS analysis

### V.5.1 Brief introduction of rare earth elements (REE)

Rare earth element (REE) means yttrium (Y) and scandium (Sc) and all the lanthanide series of elements (15 elements in total). The content of various REE elements in sedimetary rocks is contributed to the sedimentary detrital inputs and diagenesis conditions (Zwicker et al., 2018), when the rocks were formed. The REE chemical analysis is widely utilized to reconstruct the paleo-environments nowadays (Chen and Liu, 2020; Xu et al., 2009). In this study, by the ICP-MS analysis, the analysis of the REE contents would also be used to shed light on the paleo-environmental conditions of the samples collected in the Praia do Areia do Mastro site and Boca do Chapim site.

All the REE contents data in patterns, which is illustrated in this study, would be upper continental crust (UCC)-normalized through using the values given by Rudnick and Gao (2014). These REE contents data and UCC-normalized REE patterns of the samples would depict the more clear information about how these samples were formed.

### V.5.2 The samples of the Praia do Areia do Mastro site

The REE content and the UCC-normalized REE patterns of the samples collected from the Boca do Chapim site are shown on the table 5.5.2.1 and diagram 5.5.2.1, respectively.

| Sample ID / Element | PS1 | PS2 | PS3 | PS5 | PS7 | PS8 |
|---|---|---|---|---|---|---|
| Rb | 58,124 | 3,346 | 12,830 | 4,786 | 8,577 | 5,797 |
| Sr | 45,632 | 9,943 | 3,032 | 20,202 | 26,002 | 9,863 |
| Y | 8,104 | 1,799 | 0,439 | 2,755 | 1,236 | 2,135 |
| Zr | 104,035 | 53,390 | 4,678 | 11,577 | 8,617 | 14,970 |
| Nb | 7,853 | 4,143 | 0,395 | 1,285 | 0,660 | 0,861 |
| La | 12,387 | 0,600 | 2,107 | 2,067 | 2,658 | 2,082 |
| Ce | 33,936 | 10,565 | 1,468 | 6,205 | 5,028 | 6,740 |
| Pr | 4,085 | 1,307 | 0,171 | 0,708 | 0,604 | 0,792 |
| Nd | 15,122 | 4,805 | 0,645 | 2,670 | 2,326 | 2,954 |
| Sm | 2,861 | 0,893 | 0,114 | 0,468 | 0,450 | 0,546 |
| Eu | 0,510 | 0,024 | 0,080 | 0,066 | 0,142 | 0,106 |
| Gd | 2,141 | 0,627 | 0,086 | 0,444 | 0,349 | 0,486 |
| Tb | 0,346 | 0,102 | 0,015 | 0,072 | 0,057 | 0,082 |
| Dy | 1,597 | 0,442 | 0,073 | 0,348 | 0,261 | 0,388 |
| Ho | 0,320 | 0,085 | 0,014 | 0,075 | 0,050 | 0,080 |
| Er | 0,889 | 0,237 | 0,041 | 0,207 | 0,135 | 0,209 |
| Tm | 0,163 | 0,044 | 0,006 | 0,034 | 0,023 | 0,035 |
| Yb | 0,761 | 0,033 | 0,111 | 0,110 | 0,159 | 0,121 |
| Lu | 0,167 | 0,046 | 0,006 | 0,032 | 0,022 | 0,032 |
| Hf | 2,725 | 1,550 | 0,128 | 0,292 | 0,249 | 0,432 |
| Ta | 1,868 | 0,649 | 0,114 | 0,828 | 0,187 | 0,225 |
| Th | 5,520 | 0,351 | 1,214 | 0,375 | 0,881 | 0,628 |
| U | 1,642 | 0,157 | 0,571 | 0,156 | 0,314 | 0,244 |

The unit of the element's content is in the ppm.

Table 5.5.2. 1, The REE's contents of the samples from the Praia do Areia do Mastro site.

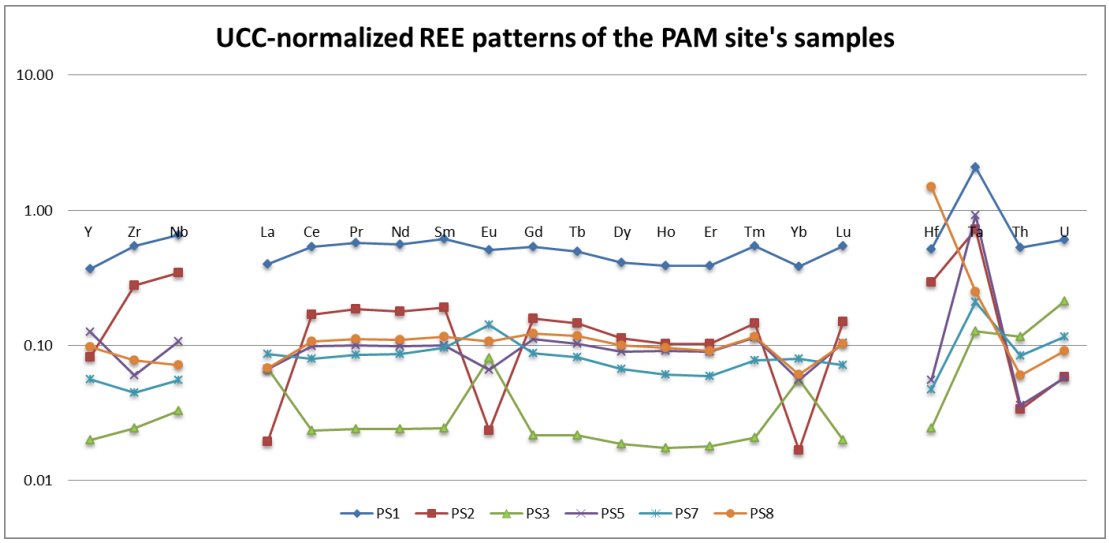


**Diagram 5.5.2. 1, The UCC-normalized REE patterns of the samples collected from the Praia do Areia do Mastro site.**

For the sample PS8, its line slight decreases from Y to Nd (neodymium). After a small growth between La (lanthanum) to Ce (cerium), the line almost level out and remain steady from Ce to Lu (lutetium); however, there is a small drop on the Yb (Ytterbium) point. After a dramatic fall from Hf (Hafnium) to Th (thorium), the line slightly grow between Th and U (uranium).

For the sample PS7, its line almost shows a small fluctuation or remain steady from Y to U, but there are two obvious peaks on the Eu and Ta (tantalum) points.

For the sample PS5, its line shows a small fall on the Zr (zirconium) point which is between Y and Nd. the line almost level out and remain steady from Ce to Lu; however, there are small drops on the Eu and Yb points.

For the sample PS3, it shows a slight growth between Y and Nd. Except the high peaks on the La, Eu and Yb points, the line almost level out and remain steady from

Ce to Lu. Between Hf and Ta, the line jumps suddenly, and remain stable from Ta to Th. The line rises slightly from Th to U.

For the sample PS2, its line jump dramatically from Y to Zr, and then slightly rise from Zr to Nd. Except the deep falls on the La, Eu and Yb points, the line almost level out and remain steady from Ce to Lu. A small growth is shown between Hf and Ta, and then the line pluments from Ta to Th. The line finally slightly increases from Th to U.

For the sample PS1, its line just increases slightly from Y to Nd. This line almost shows a small fluctuation or remain steady from La to U, but there is an obvious peak on the Ta point.

## V.5.3 The samples of the Boca do Chapim site

The REE content (table 5.5.3.1 for the samples no. 1 to 5, and table 5.5.3.2 for the samples no. 6 to 11) and the UCC-normalized REE patterns (Digaram 5.5.3.1) of the samples collected from the Boca do Chapim site are shown below.

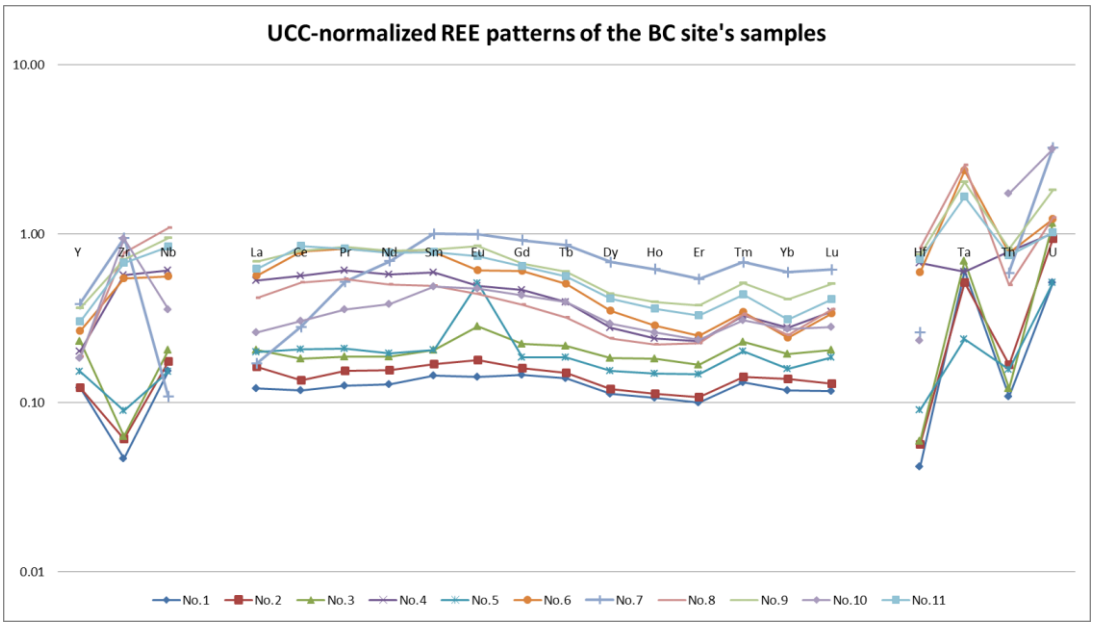


**Diagram 5.5.3. 1, The UCC-normalized REE patterns of the samples collected from the Boca do Chapim site.**

| Sample ID / Element | No. 1 | No. 2 | No. 3 | No. 4 | No. 5 |
|---|---|---|---|---|---|
| Rb | 11,823 | 18,240 | 25,405 | 57,011 | 35,869 |
| Sr | 173,546 | 156,006 | 176,715 | 22,559 | 89,293 |
| Y | 2,707 | 2,691 | 5,092 | 4,431 | 3,352 |
| Zr | 8,982 | 11,735 | 12,190 | 109,837 | 17,307 |
| Nb | 1,845 | 2,111 | 2,465 | 7,289 | 1,842 |
| La | 3,758 | 5,046 | 6,387 | 16,453 | 6,213 |
| Ce | 7,416 | 8,518 | 11,491 | 35,613 | 13,043 |
| Pr | 0,892 | 1,097 | 1,333 | 4,297 | 1,481 |
| Nd | 3,459 | 4,213 | 5,050 | 15,557 | 5,297 |
| Sm | 0,678 | 0,794 | 0,968 | 2,776 | 0,963 |
| Eu | 0,142 | 0,179 | 0,283 | 0,492 | 0,508 |
| Gd | 0,585 | 0,641 | 0,893 | 1,861 | 0,744 |
| Tb | 0,097 | 0,106 | 0,151 | 0,277 | 0,129 |
| Dy | 0,440 | 0,471 | 0,715 | 1,085 | 0,602 |
| Ho | 0,088 | 0,094 | 0,152 | 0,199 | 0,124 |
| Er | 0,231 | 0,248 | 0,387 | 0,533 | 0,339 |
| Tm | 0,040 | 0,043 | 0,069 | 0,098 | 0,060 |
| Yb | 0,237 | 0,277 | 0,390 | 0,558 | 0,318 |
| Lu | 0,036 | 0,040 | 0,064 | 0,107 | 0,057 |
| Hf | 0,222 | 0,299 | 0,315 | 3,548 | 0,479 |
| Ta | 0,543 | 0,463 | 0,620 | 0,536 | 0,214 |
| Th | 1,141 | 1,759 | 1,272 | 8,263 | 1,645 |
| U | 1,386 | 2,534 | 3,131 | 2,716 | 1,388 |

The unit of the element's content is in the ppm.

Table 5.5.3. 1, The REE's contents of the samples no. 1 to 5 from the Boca do Chapim site.

| Sample ID / Element | No. 6 | No. 7 | No. 8 | No. 9 | No. 10 | No. 11 |
|---|---|---|---|---|---|---|
| Rb | 48,253 | 11,670 | 73,727 | 80,768 | 3,303 | 66,394 |
| Sr | 24,567 | 13,701 | 25,620 | 33,223 | 1,650 | 29,624 |
| Y | 5,815 | 8,440 | 4,115 | 7,998 | 4,028 | 6,615 |
| Zr | 104,990 | 182,645 | 148,189 | 135,847 | 180,576 | 129,320 |
| Nb | 6,714 | 1,309 | 12,952 | 11,345 | 4,261 | 10,026 |
| La | 17,477 | 5,292 | 12,880 | 21,166 | 8,051 | 19,076 |
| Ce | 49,387 | 17,721 | 32,425 | 49,877 | 19,216 | 53,138 |
| Pr | 5,808 | 3,691 | 3,832 | 5,959 | 2,532 | 5,780 |
| Nd | 20,909 | 18,632 | 13,528 | 21,416 | 10,392 | 20,798 |
| Sm | 3,669 | 4,687 | 2,304 | 3,809 | 2,280 | 3,668 |
| Eu | 0,609 | 0,989 | 0,439 | 0,848 | 0,474 | 0,733 |
| Gd | 2,416 | 3,660 | 1,523 | 2,663 | 1,733 | 2,558 |
| Tb | 0,354 | 0,601 | 0,224 | 0,417 | 0,276 | 0,391 |
| Dy | 1,361 | 2,650 | 0,937 | 1,714 | 1,145 | 1,609 |
| Ho | 0,236 | 0,512 | 0,183 | 0,326 | 0,216 | 0,298 |
| Er | 0,574 | 1,243 | 0,520 | 0,868 | 0,539 | 0,753 |
| Tm | 0,103 | 0,204 | 0,100 | 0,153 | 0,092 | 0,130 |
| Yb | 0,485 | 1,182 | 0,504 | 0,819 | 0,546 | 0,621 |
| Lu | 0,105 | 0,190 | 0,111 | 0,156 | 0,087 | 0,127 |
| Hf | 3,140 | 1,383 | 4,338 | 3,976 | 1,235 | 3,725 |
| Ta | 2,137 | 0,000 | 2,283 | 1,828 | 0,000 | 1,492 |
| Th | 8,119 | 6,168 | 5,224 | 8,536 | 18,148 | 7,768 |
| U | 3,291 | 8,765 | 3,368 | 4,914 | 8,543 | 2,736 |

The unit of the element's content is in the ppm.

Table 5.5.3. 2, The REE's contents of the samples no. 6 to 11 from the Boca do Chapim site.

In this section, the samples collected from the Boca do Chapim site would be classified as three groups, which are based on their grain size and geochemical compositions, to do the discussion and comparison of their REE contents –

- Mudstone: Samples no. 11, 9, 8, 6 and 4
- Lignite: Sample no. 10 and 7
- Limestone and sandstone with several calcium carbonate: Sample no. 5, 3, 2 and 1

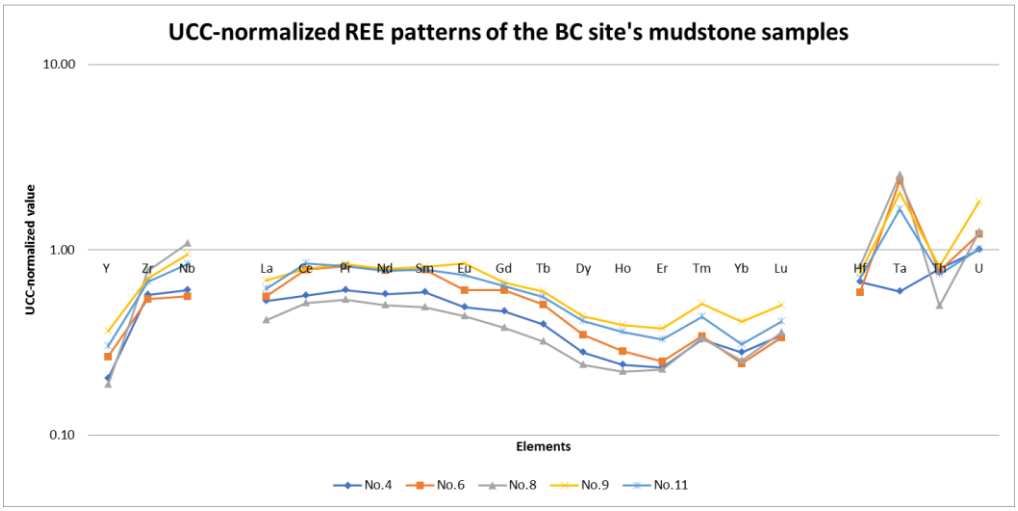


**Diagram 5.5.3. 2, The UCC-normalized REE patterns of the mudstone samples collected from the Boca do Chapim site.**

For the group of mudstone samples, the shape of the their UCC-normalized REE patterns diagram (Diagram 5.5.3.2) is described below – In general, their lines dramatically climb from Y to Zr, and from Zr Nb, they just increase slightly. From La to Eu, their lines almost level out or show small fluctuations, but from Gd to Er, the lines decline gradually. From Er to Tm, the lines gradually climb and then represent slight fluctuations between Tm and Lu. From the Hf to Ta, the lines of the samples no.11, 9, 8 and 6 increased suddenly, but the line of the sample no.4 just decreases slightly. From Ta to Th, the lines of the samples no.11, 9, 8 and 6 fall drastically, and

then climb significantly from Th to U. However, the line of the sample no.4 just shows a gradual and small increase from Ta to U.

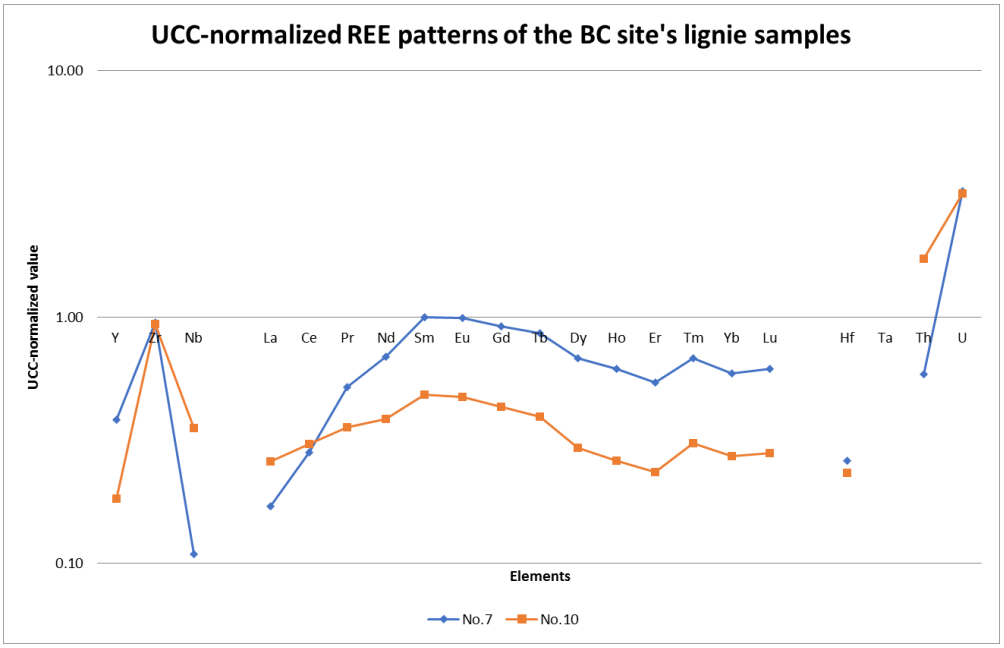


**Diagram 5.5.3. 3, The UCC-normalized REE patterns of the lignite samples collected from the Boca do Chapim site.**

For the group of lignite samples, the shape of the their UCC-normalized REE patterns diagram (Diagram 5.5.3.3) is described below – In general, from Y to Zr, there are sudden increases and then sudden drops are shown from Zr to Nb. From La to Sm, the sample no.7's line climbs significantly, but the sample no.10's line just increases slightly. Both of the lines almost leveled out and remained steady from Sm to Eu. Both of them shows gradual decrease between Eu and Er, and then slightly increase from Er to Tm. Between Tm to Lu, the lines both represent a small fluctuations. Between Lu to Hf, the sample no.7's line shows a very huge drop, but the sample no.10 just represents a small decrease. Both of lines has a very large increase from Th to U. These two samples have no Ta contents.

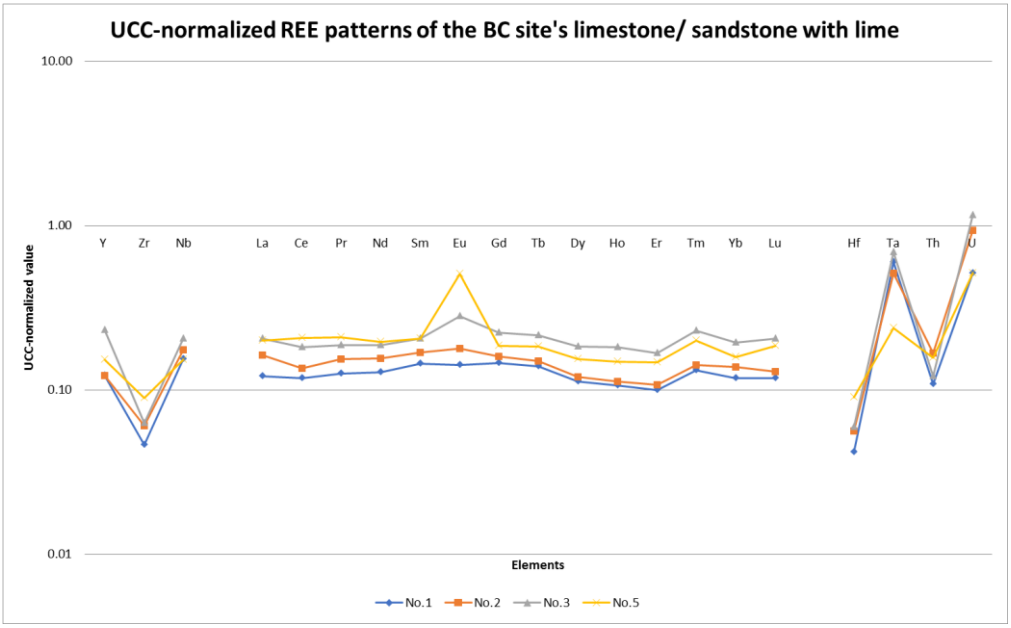


**Diagram 5.5.3. 4, The UCC-normalized REE patterns of the Boca do Chapim site's samples of limestone and sandstone with several calcium carbonate.**

For the group of the samples of limestone and sandstone with several calcium carbonate, the shape of the their UCC-normalized REE patterns diagram (Diagram 5.5.3.4) is described below – In general, from Y to Zr, there are sudden drops and then sudden growths are shown from Zr to Nb. Except that the sample no.5 and 3 have a big and small peaks, respectively, on the Eu point, the samples' lines almost just have very small fluctuations between La and Lu. All these samples' lines show significant growth from Hf to Ta, and large drops from Ta to Th. These lines then climb suddenly from Th to U.

# VI. Discussion

## VI.1 Brief introduction of sedimentary environment and evaporites of lagoon

Most of the samples in this study show the typical characteristics of lagoon sedimentary deposits. This section briefly introduce the two models of lagoon sedimentary environmental and evaporites, which are commonly found in this kind of environment.

Since the seawater inputs are generally much more than the outputs in the lagoon, after long-periodic evaporation, the significant dense salt and ion contents would be kept in the water of the lagoon environment, and then form the so-called evaporites as sedimentary deposits. The lagoon evaporites contain carbonate salts (ex. calcium carbonate), sulfate salts (ex. gypsum), halite salts and so on (Sonnenfeld, 2001). The closed lagoon environment (Fig. 6.1.1b) tends to be more anoxic than the open lagoon environment (Fig. 6.1.1a), given that the open lagoon environment has more ocean inputs, which would bring more oxic seawater, than the closed one. In the anoxic closed environment, because of the low probability of existence of the bacteria, sedimentary deposits consisting of sulfates, sulfurs, and organic matters would easily to be kept (Babel and Schreiber, 2014). In several paleontological investigations (Suarez and Bell, 1987), there are high opportunities to discover the dinosaurs' track site in the paleo-lagoon sedimentary environment.

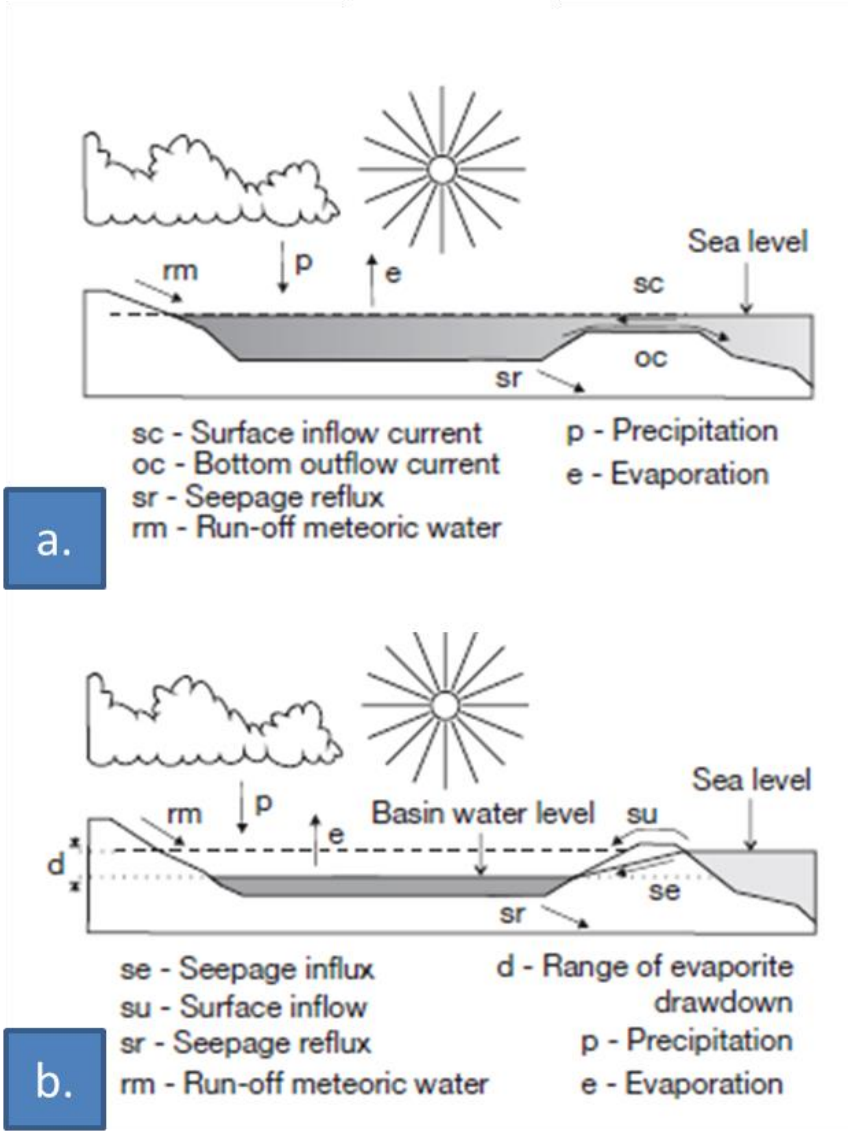


Fig. 6.1. 1, Principal models of evaporite situations in two different kinds of lagoon. (a) Open lagoon (which can also be called as the marginal marine evaporite basin of the lagoon). (b) Closed lagoon (which can also be called as the marginal marine evaporite basin of salina type). (Babel and Schreiber, 2014)

VI.2 Praia do Areia do Mastro site

The diagrams of the summarized data of the Praia do Areia do Mastro site is depicted on the diagram 6.2.1.

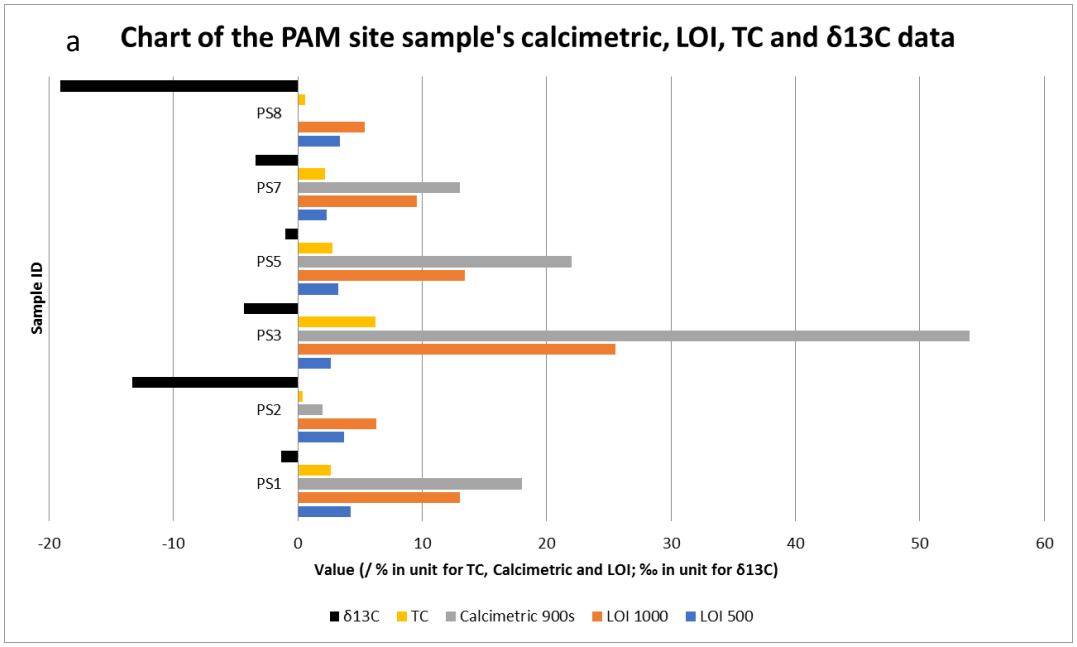


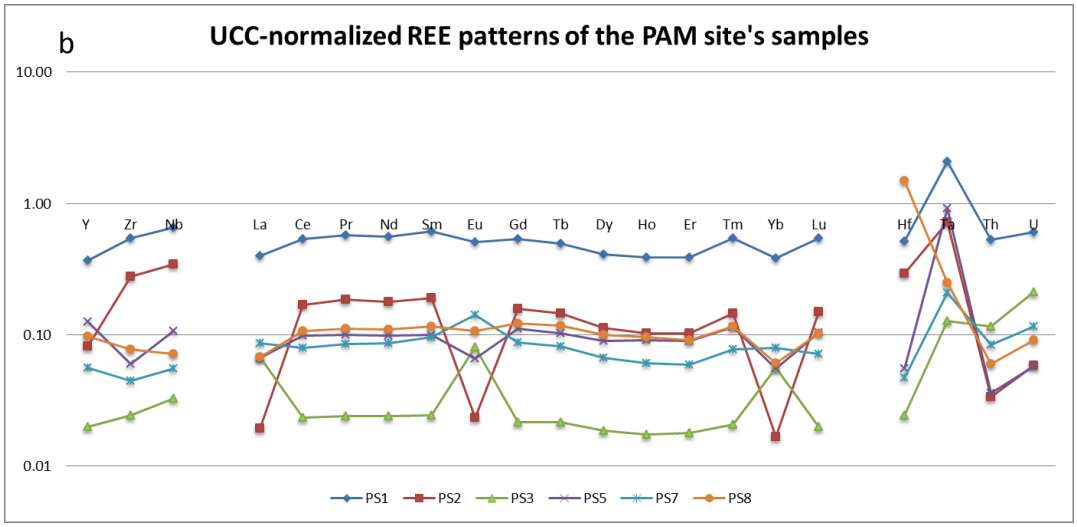


**Diagram 6.2 1, Diagrams summarize the Praia do Areia do Mastro site's samples' data in this study. (a) Bar chart of the LOI, calcimetric and $\delta^{13}C$, TC analysis reults. (b) Line graph of the UCC-normalized REE patterns of the Praia do Areia do Mastro site's samples.**

The negative $\delta^{13}C$ (Diagram 6.2.1a) value indicated all the samples collected from the Praia do Areia do Mastro site were not formed in marine but intertidal environments. The fact that there are also dinosaurs' footprints and no obvious small sea shells or corals fossils found in the microscopic observations and investigation of Figueiredo and his colleagues (2022a) can also support this viewpoint. Considering the sedimentary grain sizes and chemical compositions of all the samples, except that the sample PS1 was formed in the estuary environment due to its sandy sediments, most of the other samples of this site were probably formed in the lagoon paleo-environments; nevertheless, the temperature and capacity of oxygen in the water were various in the paleo-environment where those samples were formed.

Considering the sedimentary grain sizes and chemical compositions of the sample PS1, this sample was formed in the estuary environment and the samples PS2 and PS3 were formed in the intertidal open lagoon environments. However, from the the sample PS1's environmental condition to the sample PS2's environmental condition, there is a self-evident loss of carbonates contents, and from sample PS2's environmental condition to the sample PS3's, the content of carbonates in the samples increase again. The growth of temperature during the environmental changes between the sample PS1 and PS2 could explain this content difference of carbonates, since the high temperature environment is not easy to cause the carbonate solution to precipitate to be the minerals or salts. The Eu and Yb patterns changes on the diagram 6.1.1 also confirm this speculation. The Eu and Yb commonly precipitate with the calcite when the recrystallization of calcite happens (Hellebrandt et al., 2016). It could explain the reason why the huge gap of the Eu- and Yb points of the sample PS2's REE patterns and the peak of the the Eu- and Yb points of the sample PS3's REE patterns that the calcites in the samples tended to be dissolved from the sample PS1's

environmental condition to the sample PS2's due to the warmer climate, and then the calcites tended to precipitate from the the sample PS2's environmental condition to the sample PS3's due to the colder climate.

Considering the sedimentary grain sizes and chemical compositions of the samples PS5, this sample was formed in the open lagoon environment, because its oxic conditions caused several calcium carbonates precipitating on the muddy deposit of this sample. However, during the development of the period between the sample PS5 and PS7, the temperature of this site seemed to slight grown again, because the contents of precipitating calcium carbonate became less clearly. In the diagram 6.2.1b, peaks on the Eu- and Yb-positions in the REE patterns of the sample PS5 and the gaps of the same elements' positions in the patterns of the PS7 could confirm this speculation about temperature changes.

Considering that there are no carbonates and very low content of carbon matters in the sample PS8, it could indicate that this sample was formed in the warm closed lagoon environment, since the warm and closed water environment would inhibit the oxygen input from the sea water and dissolved in it, as well as cause the accumulation of muddy deposits. In the diagram 6.1.1b, it could also confirm this speculation about the temperature changes that the change of the sample PS7's Eu and Yb peaks in its patterns disappears when the sedimentary conditions develop to the sample PS8's environmental condition.

## VI.3 Boca do Chapim site

The diagrams of the summarized data of the Praia do Areia do Mastro site is depicted on the diagram 6.3.1.

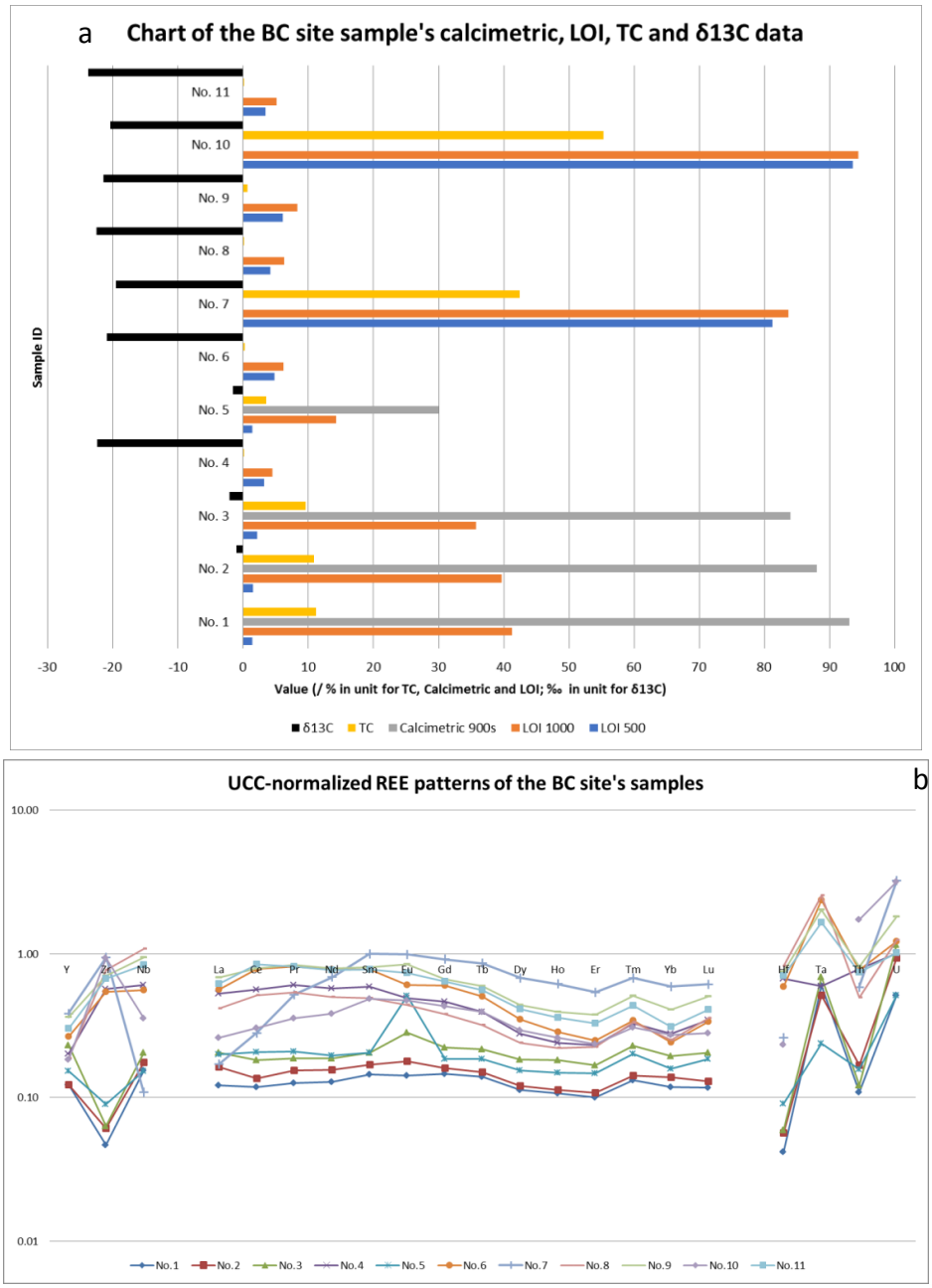


**Diagram 6.3 1, Diagrams summarize the Praia do Areia do Mastro site's samples' data in this study. (a) Bar chart of the LOI, calcimetric and $\delta^{13}C$, TC analysis reults. (b) Line graph of the UCC-normalized REE patterns of the Boca do Chapim site's samples.**

The negative $\delta^{13}C$ (Diagram 6.3.1a) value indicated all the samples collected from the Boca do Chapim site were not formed in marine but intertidal environments. The fact that there are also dinosaurs' footprints and no obvious small sea shells or corals fossils found in the microscopic observations and investigation of Figueiredo and his colleagues (2022b) can also support this viewpoint. Considering the sedimentary grain sizes and chemical compositions of all the samples, the samples no.1, 2, 3 and 5 were probably formed in the open intertidal estuary or open lagoon environment, and the samples no.4 and no.6 to 11 were formed in the lagoon. The samples no.7 and 10 were particularly obviously formed in closed lagoon, which were anoxic environment.

Considering the sedimentary grain sizes and chemical compositions of the samples no.1, 2 and 3, this sample was formed in the estuary environment, but the climates became warmer and warmer from the sample no.1's environmental condition to the sample no.3's condition. The gradually decline of the carbonates content, closed organic/ inorganic carbon compositions (Diagram 6.3.1a) and similar REE patterns (Diagram 6.3.1b) of these samples could also prove this inference.

Considering the sedimentary grain sizes and chemical compositions of the samples no.3 and 4, the sedimentary conditions had changed to be closed lagoon from the sample no.3's environmental condition to the sample no.4's, since the significant carbonates content (Diagram 6.3.1a) of the sample no.3 was not kept in the sample no.4. In the diagram 6.3.1b, the content of the light rare elements (LREE, which includes in La, Ce, Pr, Nd, Sm and Eu.) grew significantly from the sample no.3's environmental condition to the sample no.4's, could also represent the different sedimentary inputs of these two samples. Since the terrigenous sedimentary deposits commonly contain high content of the LREE (Zhang and Shields, 2022), the LREE

content difference between the sample no.3 and no.4 could depict that the sample no.3‘s mixture of marine and river sandy sedimentary inputs had be replaced as the sample no.4’s terrigenous muddy inputs. The terrigenous muddy inputs are common to appear in the closed lagoon sedimentary environment.

Considering the sedimentary grain sizes and chemical compositions of the sample 5, the sedimentary conditions had changed to be mainly the intertidal river fan, because the muddy sedimentary deposits of the sample no.4 was replaced by the sandy sedimentary deposits of the sample no.5. The rich contents of the calcium carbonate (Diagram 6.3.1a), Eu and Yb elements (Diagram 6.3.1b) indicate that there are numerous terrigenous calcites which came from river inputs in the sample no.5’s environment.

Considering the sedimentary grain sizes and chemical compositions of the samples no.6 to 11, the environments of these samples were all lagoon, since there are relatively rich sulfur and organic carbon matters and almost no calcium carbonate contents in them. The almost same REE patterns of the sample no.6, 8, 9 and 11 could also confirm this environmental hypothesis. However, the sedimentary environments of the sample no.7 and 10 were obviously anoxic closed lagoon, given that these samples are composed of lignite and gypsum, which were evaporites and easy to appear in the anoxic closed lagoon. The high content of the samples no.7’s and 10’s LREE in the diagram 6.3.1b shows that there were majorly terrigenous and almost no marine sediments in these the environments of the sample no.7 and 10.

VI.4 Probable effects to cause the paleo-environmental changes in these sites

Early Cretaceous (or called as the Lower Cretaceous) life and the environment were strongly influenced by the accelerated break up of Pangaea, which was associated with the formation of a multitude of rift basins, intensified spreading, and important volcanic activity on land and in the sea. These processes likely interacted with greenhouse conditions, and Early Cretaceous climate oscillated between “normal”, predominantly arid conditions, and intensified greenhouse, predominantly humid conditions. Arid conditions were important during the latest Jurassic and early Berriasian, the late Barremian, and partly also during the late Aptian. Arid conditions were associated with evaporation, low biogeochemical weathering rates, low nutrient fluxes, and partly stratified oceans, leading to oxygen depletion and enhanced preservation of laminated, organic-rich mud (LOM) (Follmi, 2012). The Praia Areia do Mastro and Boca do Chapim Sequences are dated in the Barremian, charaterised by arid condition. The figure 6.4.1 shows the hypothetical models mentioned in this paragraph.

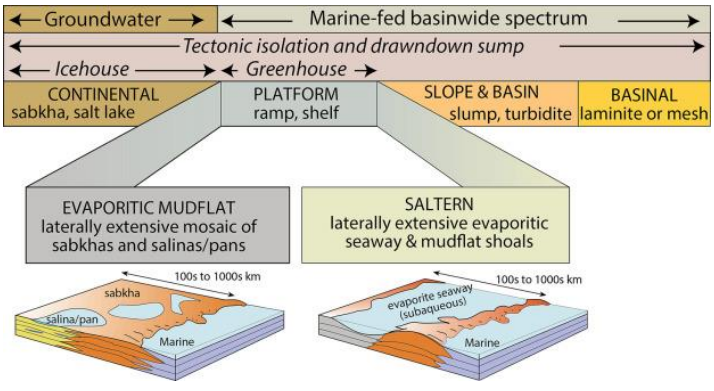


**Fig. 6.4 1, The hypothetical models show how the tectonic motions and climatic changes cause the landform changes of intertidal, estuarine and lagoon regions. (Warren, 2021)**

In accordance with Sonnenfeld's work (2001), the sequence of primary evaporite deposits proceeds from calcium carbonates (aragonite and calcite) to gypsum, such as the samples no. 7 and 10, which have been found in the sequence of the Boca do Chapim. Increasing salinity, in fact, means decreasing oxygen solubility and the carbonates take on a finely laminated texture.

The progressive concentration of the longshore current leads to a loss of carbonate ion solubility, a retreat of carbonate sedimentation near the entrance in the lagoon, and the continued deposition along the shores even after the brine in the lagoon center has reached a concentration in excess of carbonate saturation. The stripping of carbonate ions aids gypsum precipitation. The diagram 6.4.1 illustrates the effects mentioned in this paragraph.

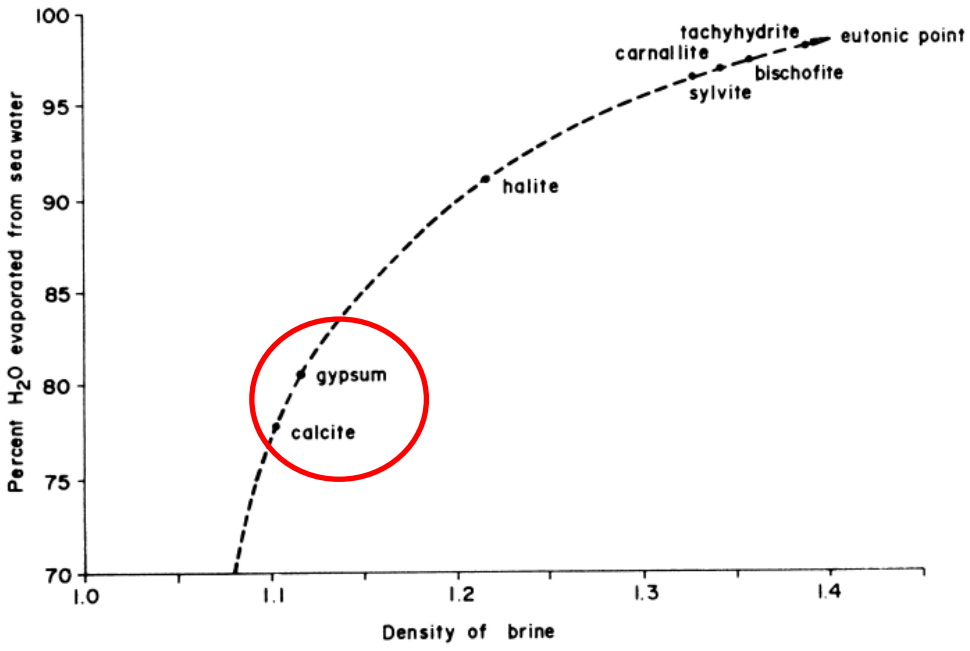


Diagram 6.4. 1, The diagram shows the relationship between the brine density changes and the percentage of water which evaporated from the sea. (Sonnenfeld, 2001)

In particular, as regards the Boca do Chapim site's samples 7 and 10, Sonnenfeld (2001) suggest that two environments provide for a large-scale accumulation of organic matter under the exclusion of atmospheric oxygen: deltas and evaporite basins. Both deltaic sediments and evaporites forming density-stratified basins with anaerobic Eh-negative bottom brines; they are marked by high rates of subsidence and rapid sediment accumulation, and by high biomass productivity in surface waters.

In the case of Boca do Chapim sequences, both of these conditions were satisfied, in deltaic environments, the organic matter can be trapped in clayey deposits and anoxic waters of normal salinity contain only two to three times the concentration of both soluble and particulate organic carbon compared to open ocean waters. If more organic matter is found in the bottom sediments, it indicates faster rates of accumulation rather than slower rates of decomposition in an anaerobic environment. In brines of evaporite basins, the organic matter can attain much higher values.

# VII. Conclusion

This study, which is part of the research that has already been going on for years in the Espichel Cape area, more specifically in the areas of the Paia Areia do Mastro and Boca do Chapim, where important paleontological discoveries have been made, sought to provide, through microscopic, geochemical and isotopic analyses, a more complete picture of the paleo-environmental conditions in this region during the Barremian (Lower Cretaceous).

The breakup of Pangaea in the Early Cretaceous strongly affected life and the environment and the climatic condition oscillated between “normal” predominantly arid conditions and intensified greenhouse, predominantly humid conditions.

The samples of this study, collected from the Praia Areia do Mastro and the Boca do Chapim sites in the Espichel Cape area, are dated in the Barremian when arid conditions were associated with evaporation, low biogeochemical weathering rates, low nutrient fluxes, and partly stratified oceans, leading to oxygen depletion and enhanced preservation of laminated, organic-rich mud.

In fact, the microscopic observations and the chemical analyses in this study have permitted to highlight a rough picture of the development of the Lower Cretaceous lagoon and estuary environments and temperature changes in the Praia do Areia do Mastro and Boca do Chapim sites.

In this study, microscopic observations on stereomicroscope have been associated with calcimetric and LOI determination, 13C stable isotope and Rare Earth Elements

content analyses.

As regards the Praia Areia do Mastro the observations and the analyses permitted to depict of an area characterized by alternation between marginal marine siliciclastic environments and shallow marine carbonate environments, which were present in estuarine conditions with various exchange of water inputs from the ocean and rivers.

As concerns, the Boca do Chapim site the data collected from the microscopic observations of the samples and the analyses led to hypothesize that the paleo-environment was very similar to those suggested for Praia Areia do Mastro site, with marine/estuarine environment with siliciclastic to carbonate mixed brackish lacustrine system due to occasional marine incursions. These conditions were favorable for the formation of not too many extended evaporite basins where, due to an adequate supply of decomposing organic matter, the evaporite-precipitating brines were able to generate large amounts of potential hydrocarbons without the necessity to first keep them locked in an impervious bed.

# VIII. Acknowledgments

The author would like to thank Prof. Pedro Cunha in the University of Coimbra, Portugal, Antonello Aquilano, and the technicians in the Department of Environment and Prevention Sciences and Department of Physics and Earth Science in the University of Ferrara. Prof. Cunha's suggestion and guides better the stratigraphic description and discussion of the sedimentary samples' data in this thesis. Antonello Aquilano, the doctoral candidate in the Department of the Architecture, and the technicians, Dr. Umberto Tessari and Dr. Renzo Tassinari, in the Department of Physics and Earth Science in the University of Ferrara assisted the preparation and technical supports of the ICP-MS and IRMS analysis. Because of their helps, this work could be complicated successfully.

# IX. Reference


Aillud, G. S. 2001. “Palaeoecology, Palaeoenvironmental Analysis and Their Application to Sequence Stratigraphy: Lower Cretaceous, Lusitanian Basin, Portugal.” University of Plymout; Plymouth, United Kingdom.

Antunes, M. T. 1976. “Dinossáurios Eocretácicos de Lagosteiros” Ciências da Terra; Universidade Nova de Lisboa; Lisboa, Portugal.

Babel, M., and B. C. Schreiber. 2014. “Geochemistry of Evaporites and Evolution of Seawater.” In *Treatise on Geochemistry*, edited by H. D. Holland and K. K. Turekian, 2nd ed., 9:483–560. Elsevier Ltd. .

Chen, Y., and J. Liu. 2020. “Review on the Research of Rare Earth Elements in Microbialites.” *Acta Palaeontologica Sinica* 59 (4): 499–511.

Coimbra, R., A. C. Azeredo, M. C. Cabral, and A. Immenhauser. 2016. “Palaeoenvironmental Analysis of Mid-Cretaceous Coastal Lagoonal Deposits (Lusitanian Basin, W Portugal).” *Palaeogeography, Palaeoclimatology, Palaeoecology* 446: 308–25.

Dutta, K., E. A. G. Schuur, J. C. Neff, and S. A. Zimov. 2006. “Potential Carbon Release from Permafrost Soils of Northeastern Siberia.” *Global Change Biology* 12: 1–16.

Figueiredo, S., P. Rosina, and L. Figuti. 2015. “Dinosaurs and Other Vertebrates from the Papo-Seco Formation (Lower Cretaceous) of Southern Portugal.” *Journal of Iberian Geology* 41 (3): 301–14.

Figueiredo, S., I. B. Strantzali, P. Rosina, and M. Gomes. 2016. “New Data about the Paleo-environment of the Papo-Seco Formation (Lower Cretaceous) of Southern Portugal.” *Journal of Environmental Science and Engineering A* 5: 463–70.

Figueiredo, S., P. Dinis, J. Belo, P. Rosina, and I. B. Strantzali. 2017. “A New Record of a Possible Ornithopod Footprint from the Lower Cretaceous of Cabo Espichel (Sesimbra, Portugal) Silvério.” *Bollettino Della Societa Paleontologica Italiana* 56 (2): 217–31.

Figueiredo, S., P. Rosina, I. B. Strantzali, V. Antunes, and S. Figueiredo. 2020. “Paleoenvironmental Approach on the Lower Cretaceous Sequences of Areia Do Mastro (Cabo Espichel, Southern Portugal).” *Journal of Environmental Science and Engineering A* 9: 66–71.

Figueiredo, S., C. N. Carvalho, P. P. Cunha, and I. S. Carvalho. 2021. “New Dinosaur Tracks from the Lower Barremian of Portugal (Areia Do Mastro Formation, Cape Espichel).” *Journal of Geoscience and Environment Protection* 09: 84–96.

Figueiredo, S, I. S. Carvalho, X. Pereda-Suberbiola, P. P.Cunha, V. Antunes, and I. Diaz-Martinez. 2022a. “New Ornithopod Footprints from the Areia Do Mastro Formation (Lower Cretaceous), Espichel Cape (Portugal, Western Iberia) and Their Context in the Iberian Ichnological Ornithopod Record.” *Cretaceous Research* 131.

Figueiredo, S., P. P.Cunha, X. Pereda-Suberbiola, C. N. Carvalho, I. S. Carvalho, E. Buffetaut, H. Tong, M. F. Sousa, V. Antunes, and R. Anastacio. 2022b. “The Dinosaur Tracksite from the Lower Barremian of Areia Do Mastro Formation (Cabo Espichel, Portugal): Implications for Dinosaur Behavior.” *Cretaceous Research* 137.

Follmi, K. B. 2012. “Early Cretaceous Life, Climate and Anoxia.” *Cretaceous Research* 35: 230–57.

Hellebrandt, S. E., S. Hofmann, N. Jordan, A. Barkleit, and M. Schmidt. 2016. “Incorporation of Eu(III) into Calcite under Recrystallization Conditions.” *Scientific Reports* 6: 1–10.

Kusaka, S., and T. Nakano. 2014. “Carbon and Oxygen Isotope Ratios and Their Temperature Dependence in Carbonate and Tooth Enamel Using Gas Bench II Preparation Device.” *Rapid Communications Mass Spectrometry* 28: 563–67.

Lapparent, A. F. de, G. Zbyszewski. 1957 “Les dinosauriens du Portugal. ” In *Memórias dos Serviços Geológicos de Portugal*, 63, Lisboa, Portugal.

Lindholm, R.C. 1988. “Sedimentary Rocks, Field Relations.” In *The Encyclopedia of Field and General Geology*, 764–74. Boston, USA: Springer.

Papeschi, S. 2022. “Geology Is the Way.” Geology Is the Way. 2022. www.geologyistheway.com.

Rudnick, R. L., and S. Gao. 2013. “Composition of the Continental Crust.” In *Treatise on Geochemistry: Second Edition*, edited by H. D.Holland and K. K.Turekian, 2nd ed., 4:1–51. Elsevier Ltd.

Sonnenfeld, Peter. 2001. “Evaporites.” In *Encyclopedia of Physical Science and Technology, Volume 5*, edited by Robert A. Meyers, 3rd ed., 653–70. Academic Press.

Sauvage, H. E. 1897. *Vertébres fossils du Portugal. Contribuition à l’étude des Poisson et des Reptiles du Jurrassique et Crétacique* . Dir. Trab. Geol., Portugal

Suarez, M., and C. M. Bell. 1987. “Upper Triassic to Lower Cretaceous Continental and Coastal Saline Lake Evaporites Inthe Atacama Region of Northern Chile.” *Geological Magazine* 124 (5): 467–75.

Warren, J. K. 2021. “Evaporite Deposits.” In *Encyclopedia of Geology*, edited by D. Alderton and S. A. Elias, 2nd ed., 945–77. Oxford: Academic Press.

Xu, Z., D. Lim, J. Choi, S. Yang, and H. Jung. 2009. “Rare Earth Elements in Bottom Sediments of Major Rivers around the Yellow Sea: Implications for Sediment Provenance.” *Geo-Marine Letters* 29 (5): 291–300.

Zhang, K., and Graham A. S. 2022. “Sedimentary Ce Anomalies: Secular Change and

Implications for Paleoenvironmental Evolution.” *Earth-Science Reviews* 229: 104015.

Zwicker, J., D. Smrzka, T. Himmler, P. Monien, S. Gier, J. L.Goedert, and J. Peckmann. 2018. “Rare Earth Elements as Tracers for Microbial Activity and Early Diagenesis: A New Perspective from Carbonate Cements of Ancient Methane-Seep Deposits.” *Chemical Geology* 501: 77–85.